Average versus high surface ozone levels over the continental U.S.A.: Model bias, background influences, and interannual variability

Jean J. Guo[1], Arlene M. Fiore[1], Lee T. Murray[2,3,4], Daniel A. Jaffe[5], Jordan L. Schnell[6,7], Tom Moore[8], George Milly[2]

[1]Department of Earth and Environmental Sciences and Lamont-Doherty Earth Observatory of Columbia University, Palisades, NY, U.S.A.
[2]Lamont-Doherty Earth Observatory of Columbia University, Palisades, NY, U.S.A.
[3]NASA Goddard Institute for Space Studies, New York, NY USA
[4]Now at: Department of Earth and Environmental Sciences, University of Rochester, Rochester, NY, U.S.A.
[5]University of Washington, School of STEM, Bothell, WA and Department of Atmospheric Science, Seattle, WA, U.S.A.
[6]NOAA Geophysical Fluid Dynamics Laboratory, Atmospheric and Oceanic Sciences, Princeton University, Princeton, NJ, U.S.A.
[7]Now at: Department of Earth and Planetary Sciences, Northwestern University, Chicago, IL, U.S.A.
[8]WESTAR and WRAP, Colorado State University, Fort Collins, CO, U.S.A.

Correspondence to: Jean J. Guo (jean.j.guo@columbia.edu)

Abstract. U.S. background ozone (O_3) includes O_3 produced from anthropogenic O_3 precursors emitted outside of the U.S.A., from global methane, and from any natural sources. Using a suite of sensitivity simulations in the GEOS-Chem global chemistry-transport model, we estimate the influence from individual background versus U.S. anthropogenic sources on total surface O_3 over ten continental U.S. regions from 2004-2012. Evaluation with observations reveals model biases of +0-19 ppb in seasonal mean maximum daily 8-hour average (MDA8) O_3, highest in summer over the eastern U.S.A. Simulated high-O_3 events cluster too late in the season. We link these model biases to excessive regional O_3 production (e.g., U.S. anthropogenic, biogenic volatile organic compounds (BVOC), and soil NO_x, emissions), or coincident missing sinks. On the ten highest observed O_3 days during summer (O_3_top10obs_JJA), U.S. anthropogenic emissions enhance O_3 by 5-11 ppb and by less than 2 ppb in the eastern versus western U.S.A. The O_3 enhancement from BVOC emissions during summer is 1-7 ppb higher on O_3_top10obs_JJA days than on average days, while intercontinental pollution is up to 2 ppb higher on average versus on O_3_top10obs_JJA days. During the summers of 2004-2012, monthly regional mean U.S. background O_3 MDA8 levels vary by up to 15 ppb from year to year. Observed and simulated summertime total surface O_3 levels on O_3_top10obs_JJA days decline by 3 ppb (averaged over all regions) from 2004-2006 to 2010-2012, reflecting rising U.S. background (+2 ppb) and declining U.S. anthropogenic O_3 emissions (-6 ppb) in the model. The model attributes interannual variability in U.S. background O_3 on O_3_top10obs days to natural sources, not international pollution transport. We find that a three-year

35 averaging period is not long enough to eliminate interannual variability in background O_3 on the highest observed O_3 days.

1   Introduction

In the United States, ozone (O_3) is regulated as a criteria pollutant under the National Ambient Air Quality Standard (NAAQS). The current NAAQS for ground-level O_3, set in October 2015, states that the 4th-highest daily
40   maximum 8-hour average (MDA8) O_3, averaged across three consecutive years, cannot be 71 ppb or higher (U.S. Environmental Protection Agency, 2015). The three-year average is nominally intended to smooth out fluctuations in O_3 levels resulting from natural variability in meteorology within the timing constraints of the federal Clean Air Act for air quality planning. As even one ppb of excess O_3 may be enough to push a county out of NAAQS attainment, it is relevant to understand which sources influence the severity and timing of the highest O_3 events.
45   Since measured O_3 does not retain a signature of the source from which it was produced, estimates of background O_3 rely on models, ideally evaluated closely with observations, to build confidence in the model capability for source attribution. Here we apply a global chemistry-transport model alongside O_3 observations to examine which sources are influencing average versus high-O_3 events, and the extent to which they vary from year-to-year.

As U.S. anthropogenic emissions of O_3 precursors decline, the relative importance of "U.S. background" to
50   total surface O_3 rises. U.S. background O_3 is defined here as the O_3 levels that would exist in the absence of U.S. anthropogenic emissions of O_3 precursors, nitrogen oxide (NO_x) and non-methane volatile organic compound (NMVOC). U.S. background O_3 thus includes naturally occurring O_3 as well as O_3 produced from global methane (including U.S. anthropogenic emissions) and from O_3 precursor emissions outside of the U.S.A. Jaffe et al. (2018) review the current understanding on U.S. background O_3 from models and observations, and its relevance to air quality
55   standard setting and implementation. Previous studies estimating background O_3 over the United States found that background sources of O_3, including stratospheric O_3 intrusions (Lin et al., 2012, 2015a), increasing Asian anthropogenic emissions (Lin et al., 2015b), and more frequent wildfires in summer (Abatzoglou and Williams, 2016; Jaffe, 2011; Yang et al., 2015), may present challenges to obtaining the O_3 standard, especially since regional emission controls may be offset by a warming climate (Fiore et al., 2015). At high-altitude sites in the western U.S.A. (WUS)
60   in spring, the influence from stratospheric intrusions and foreign transport, combined with relatively deep planetary boundary layers, can lead to high background O_3 events (Fiore et al., 2002; Zhang et al., 2011). Lin et al. (2017)

investigated surface O_3 trends over the U.S.A. from 1980-2014 with the GFDL AM3 model and found that emissions controls decreased the 95th percentile summer O_3 values in the eastern U.S.A. (EUS) by 5-10 ppb over 1988-2014, but rising Asian emissions increased by 2-8 ppb at individual sites in the WUS over the period (Lin et al., 2016).

Earlier work in the GEOS-Chem model analyzing background O_3 during a single meteorological year noted a tendency for the model to underestimate springtime O_3 at high-altitude WUS sites but overestimate summertime O_3 over the EUS (e.g. Fiore et al., 2002, 2003; Wang et al., 2009; Zhang et al., 2011, 2014). Identifying the extent to which these biases reflect poor representation of U.S. anthropogenic versus background O_3 sources is relevant for assessing uncertainties in estimates of background O_3 on days when the O_3 NAAQS is exceeded. We build upon prior studies by analyzing MDA8 O_3 measurements and 9-year model simulations spanning 2004-2012 from the GEOS-Chem 3D global chemistry-transport model (CTM). A suite of sensitivity simulations in which different emissions of O_3 precursors are perturbed allows us to identify which sources are contributing the most to observed high-O_3 days and on the days with the highest model bias. We assess here whether biases in the model reflect problems in the modeled transported background versus O_3 produced within the U.S. from both background and anthropogenic sources. In addition, the availability of these simulations for 2004-2012 allow us to investigate the year-to-year variability in background sources and the extent to which this variability is relevant for observed high events, and therefore, potentially to attaining the O_3 NAAQS. Though coarse resolution global models such as GEOS-Chem will mix emissions into the same grid cell that may remain separate in the real atmosphere, a global model is necessary to quantify background O_3 transported intercontinentally, including that produced via oxidation of methane. We estimate the influence from various individual background sources on O_3 concentrations and the interannual variability in background O_3 levels with a focus on the highest 10 events in each of the 10 U.S. EPA regions during each summer (JJA) or year. We aim to answer the following questions: (1) Which sources exert the strongest influence on O_3 on the ten days with the highest model biases against observations? (2) Which background sources influence total O_3 the most on average versus the 10 highest O_3 days? (3) Which sources influence the interannual variability of O_3 in each region on average versus the 10 highest O_3 days?

2   Observations and model simulations

2.1 Observations

We use observed 2004-2012 MDA8 O_3 data from the EPA Air Quality System (AQS) network of urban, suburban, and rural monitoring sites, the Clean Air Status and Trends Network (CASTNet), and the Mount Bachelor

90   Observatory

(https://digital.lib.washington.edu/researchworks/browse?type=subject&value=Mt.+Bachelor+Observatory) in

Oregon. MDA8 O_3 values for the AQS sites were downloaded from

http://aqsdr1.epa.gov/aqsweb/aqstmp/airdata/download_files.html#Daily (2004-2012 data last updated June 28,

2013). This dataset includes 1644 total sites from the contiguous U.S.A. from 2004-2012 with 1207 to 1333 sites

95   collecting data each year (U.S. Environmental Protection Agency, 2014) (Supplemental Table 1).

       The CASTNet (ftp://ftp.epa.gov/castnet/data) O_3 monitoring sites are located in rural areas away from

emission sources and densely populated regions. CASTNet sites are designed to capture background O_3 levels and

characterize broad spatial and temporal O_3 trends. We calculate the MDA8 O_3 concentration from hourly values at

108 CASTNet sites with data between 2004-2012, requiring at least 18 hours of data per day for each MDA8 O_3

100   calculation.

       The Mount Bachelor Observatory, established in 2004 by the University of Washington Jaffe Research

Group, is located 2.7 km above sea level on the summit of Mount Bachelor, an extinct volcano in the Cascade

Mountains of central Oregon. It provides an estimate of baseline O_3 levels over the West Coast of the United States.

Baseline O_3 is defined as the O_3 concentration at sites with negligible influence from local emissions (National

105   Research Council, 2010). Baseline O_3 is a measurable quantity and differs from background O_3 in that it contains

some influence from U.S. anthropogenic emissions that were not recently emitted but contributed to the global

background. This station represents variations in baseline O_3 concentrations (Baylon et al., 2016) and is analyzed as

a standalone site in Section 3.2 given the relevance of high-altitude measurements for downwind surface O_3

(Stauffer et al., 2017). We take all hourly O_3 concentrations from Mount Bachelor and calculate the MDA8 O_3

110   concentrations for 2004-2012. Daily averages are included only if at least 18 hours of data are available and monthly

averages require at least 20 days with valid 24-hour mean or MDA8 data. For our comparison to monthly average

O_3 at Mount Bachelor Observatory, we sample the model both at the level closest to 2.7 km and at the surface.

       We use temperature data from a 0.5º x 0.5º resolution gridded dataset developed by Fan and van den Dool

(2008) using data from the Global Historical Climatology Network (GHCN) and the Climate Anomaly Monitoring

115   System (CAMS). Each observational site is matched to the temperature model grid cell it falls in and the average

monthly temperature is computed by averaging across all the sites in each region.

In order to evaluate the GEOS-Chem model O_3 simulation (described below in Sect. 0) at a spatial scale comparable to the coarse horizontal resolution global grid (2° x 2.5°), we use an available 1° x 1° grid of surface MDA8 O_3 measurements, interpolated from the AQS, CASTNet, and Canadian NAPS networks (Schnell and Prather, 2017). We degrade this 1° x 1° dataset to 2° x 2.5° to match the horizontal resolution of the GEOS-Chem simulations. As we did not archive three-dimensional high frequency data, all MDA8 O_3 values from the model are sampled at the lowest surface layer for comparison to observational sites.

2.2 Analysis regions

Each observational site in the EPA AQS and CASTNet datasets is linked to one of the 10 U.S. EPA air quality regions (Supplemental Figure 1) based on which state the site is in. The Mount Bachelor data were included with Region 10 (Pacific Northwest) sites even though it is not a regulatory monitor. Following Reidmiller et al. (2009), we select two regions, the Southeast (Region 4) and Mountains and Plains (Region 8), as representative regions for the EUS and WUS for illustration purposes in the main text. Figures for the other eight regions are included in the supplement.

To find the daily mean O_3 concentration within each region, we first match each observational site to the model grid within which it falls. We then average across all sites in each region to obtain a regional mean MDA8 O_3 value in the observations and in the model. From the regionally averaged observed MDA8 O_3, we find: (1) the ten days with the highest observed O_3 during each year (hereafter, O_3_top10obs days), similar to the definition for extreme events used in Schnell et al. (2014), (2) the ten days with the highest O_3 observations during each season (hereafter, O_3_top10obs_MAM, O_3_top10obs_JJA, and O_3_top10obs_SON), and (3) the 4th highest MDA8 O_3 within each year. In addition, we sample the model to find the ten days each year with the highest positive biases. There is at most a 2-6 day overlap between the top 10 O_3_Base days and the top 10 most biased days in 2004-2012 across all regions, but during most years, the overlap is around 0-2 days. We restrict our analysis to examining the top 10 observed O_3 days as these days are most relevant from a policy perspective. We use O_3_top10obs as our primary metric, however, instead of the policy-relevant 4th highest O_3 because the model bias is typically lower on O_3_top10obs days (Supplemental Figure 2 versus Supplemental Figure 3). On the days when the 4th highest values occur, the model bias is generally more strongly negative in the west and South Central regions and more strongly positive in the Midwest than on O_3_top10obs days (Supplemental Figure 2, Supplemental Figure 3). In addition,

while the model rarely captures the exact day of the 4th highest MDA8 O_3 event, there is a 3-4 day overlap on

145 average between the $O_3\_top10obs$ days and the highest 10 MDA8 O_3 days in the model. This overlap is similar to

the 3 and 6 day overlap Jaffe et al. (2018) found in their regional models for May 1st to September 29th, 2011.

2.3 GEOS-Chem model simulations

We use the GEOS-Chem v9_02 global 3D chemical transport model (CTM) (http://www.geos-chem.org) simulations driven by Modern-Era Retrospective analysis for Research and Applications (MERRA) reanalysis

150 meteorology from the NASA Global Modeling and Assimilation Office for 2004-2012 (Rienecker et al., 2011). The

MERRA reanalysis is available at 1/2° by 2/3° horizontal resolution, which we degrade here to 2° by 2.5° horizontal

resolution. MERRA meteorology captures summer mean surface temperatures to within 1-2 K across U.S. regions

and precipitation to within 0.5 mm d^{-1} except for over the Northern Great Plains where a positive bias exceeds 1 mm

d[-1], but the variance in summer mean precipitation is lower than observed in some regions (Bosilovich, 2013). While

155 interannual variability in cloudiness observed at weather stations is largely captured by MERRA, the reanalysis

generally underestimates cloud cover and thus overestimates observed downward surface shortwave fluxes (Free et

al., 2016). Methane surface concentrations are prescribed each month using spatially interpolated surface

distributions from NOAA Global Monitoring Division flash data. We use the standard v9_02 chemical mechanism

which includes recycling of isoprene nitrates (Mao et al., 2013) in contrast to the mechanisms used in earlier versions

160 of GEOS-Chem (e.g., Zhang et al., 2014 as discussed in Fiore et al., 2014). Anthropogenic base emissions are from

the Emission Database for Global Atmospheric Research (EDGAR) version 3.2-FT2000 inventory (Olivier et al.,

2005) for inorganic compounds and the REanalysis of the TROpospheric chemical composition (RETRO) inventory

(Hu et al., 2015; Schultz, 2007) for organic compounds. Inorganic emissions are overwritten by regional inventories

for the U.S. (EPA National Emissions Inventory 2005), Canada (Criteria Air Contaminants), Mexico (Big Bend

165 Regional Aerosol and Visibility Observational study; Kuhns and Green, 2003), Europe (European Monitoring and

Evaluation Programme; Auvray and Bey, 2005), and South and East Asia (Streets et al., 2006). Separate global

inventories are used for ammonia (Bouwman et al., 1997), black carbon (Bond et al., 2007; Leibensperger et al.,

2012), and ethane (Xiao et al., 2008). Anthropogenic surface emissions have diurnal and monthly variability, some

with additional weekly cycles, and are scaled each year on the basis of economic data and estimates provided by

170 individual countries, where available (van Donkelaar et al., 2008). The model does not include daily variations in

U.S. anthropogenic emissions associated with higher electricity demand on hotter days (e.g., Abel et al., 2017).

Aircraft emissions are from the Aviation Emissions Inventory Code (AEIC) inventory (Stettler et al., 2011) and shipping emissions are from International Comprehensive Ocean-Atmosphere Data Set (ICOADS; Lee et al., 2011; Wang et al., 2008). Biomass burning emissions follow the interannually-varying monthly Global Fire Emissions Database version 3 (GFED3) inventory driven by satellite observations of fire activity (Giglio et al., 2010; Van Der Werf et al., 2010). Biofuel emissions are constant (Yevich and Logan, 2003). Biogenic VOC emissions from terrestrial plants follow the Model of Emissions of Gases and Aerosols from Nature (MEGAN) scheme version 2.1 (Guenther et al., 2012) and vary with meteorology (Barkley et al., 2011). Global and U.S. emissions are 29.5 Tg N yr^{-1} and 5.2 Tg N yr^{-1} respectively, for anthropogenic NO_x emissions (including biofuels); 4.2 Tg N yr^{-1} and 0.1 Tg N yr^{-1} for biomass burning; 8.7 Tg N yr^{-1} and 0.9 Tg N yr^{-1} for soil NOx; 6.7 Tg N yr^{-1} and 1.0 Tg N yr^{-1} for lightning NOx; 466.1 Tg C yr^{-1} and 20.6 Tg C yr^{-1} for isoprene emissions. Emissions for NO_x sources and isoprene are provided globally and within the U.S.A. for each year in Supplemental Table 3.

We first perform a base simulation (O_3_Base) with all emissions turned on for 2003-2012. We conduct a parallel suite of sensitivity simulations, in which selected sources are removed. In all simulations, we discard 2003 from our analysis as initialization. Our first set of sensitivity simulations estimates three different "background" definitions: (1) "North American Background" (denoted O_3_NAB) in which anthropogenic emissions within Canada, Mexico, and the U.S.A. are set to zero, but methane surface abundances are kept at present-day values; (2) "U.S. background" (O_3_USB), which is similar to O_3_NAB except only U.S. anthropogenic emissions are set to zero; (3) "Natural background" (O_3_NAT), in which all anthropogenic emissions have been removed globally and methane is prescribed at preindustrial levels. We estimate Canadian and Mexican influence (O_3_CA+MX) on U.S. O_3 by subtracting O_3_NAB from O_3_USB; the influence from intercontinental pollution transport plus global methane (O_3_ICT+CH_4) is estimated by subtracting O_3_NAT from O_3_NAB. A second set of sensitivity simulations enable us to estimate the contribution of individual "background" sources to total simulated surface O_3 by subtracting a simulation with that source shut off from the O_3_Base simulation: (1) O_3_NALNO$_x$ by turning off North American lightning NOx; (2) O_3_SNO$_x$ by zeroing out global soil NOx; (3) O_3_BVOC by zeroing out terrestrial biogenic VOC emissions (we also examine this "O_3_noBVOC" simulation in Section 3.3); (4) O_3_BB by zeroing-out biomass burning emissions, as summarized in Table 1. Due to non-linearities in atmospheric photochemistry, these "zero-out" estimates of source contributions depend on the presence of all other precursor emissions at present-day levels (e.g., the impact of BVOCs emissions is sensitive to the amount of anthropogenic NO_x emissions in the Base

200   simulation). This set of model simulations does not directly isolate stratospheric O_3 or Asian influences. Previous

work has shown that stratospheric O_3 can increase springtime O_3 levels by 17-40 ppb in the WUS when MDA8 O_3

levels are 70-85 ppb, and Asian emissions can contribute 8-15 ppb to MDA8 O_3 on days above 60 ppb (Lin et al.,

2012, 2015a). Stratospheric and Asian influences are included in O_3_USB; Asian influences are included in

$O_3\_ICT+CH_4$; and O_3_NAT includes stratospheric O_3, biogenic emissions of O_3 precursors, wildfires, and lightning

205   NO_x. As O_3_BVOC includes O_3 produced from biogenic VOC reacting with both natural and anthropogenic NO_x,

O_3_USA and O_3_BVOC are not additive. O_3_BVOC thus contributes to both O_3_USA and O_3_USB.

3   Model evaluation

3.1   MDA8 O_3 distributions

To evaluate the ability of our coarse resolution model to capture observed high-O_3 events, we compare the

210   MDA8 O_3 averaged over each of the 10 EPA regions simulated by GEOS-Chem to the observations in two ways. In

the first method, we use the (Schnell and Prather, 2017) gridded dataset degraded to the model resolution and

sample the model directly at each of the degraded Schnell grid cells prior to calculating the regional average. In the

second method, we sample the model grid cell containing each individual observational site (EPA AQS, CASTNet,

and Mount Bachelor Observatory) prior to calculating the regional average. The model is biased positively with

215   either method (Figure 1a, b), but the shape of the model distribution constructed with the latter approach (Figure 1b)

better matches the observed distribution than that of the former (Figure 1a). Matching individual sites to the nearest

model grid (Figure 1b) yields a better estimate of high-O_3 days; the model overestimates the percentage of days

above 70 ppb by about three times when we match to individual measurement sites (3.14% of days are above 70 ppb

in the observations versus 9.92% in model) but by about ten times in comparison to the re-gridded Schnell (2014)

220   dataset (0.37% of days are above 70 ppb in the observations versus 3.91% in the re-gridded dataset).

Simulated seasonal mean MDA8 averaged over the full 2004-2012 period is higher than observed by 5-30

ppb (Figure 2a, b, c), with the largest biases typically occurring in the Northeast and Midwest. The model bias is

highest in summer (JJA) (15-30 ppb at most sites), followed by fall (SON) (10-20 ppb) (Figure 2a, b, c). Recent

work in a newer version of GEOS-Chem attributes some of the positive model bias in the EUS to excessive NO_x

225   emissions in the 2011 National Emission Inventory (NEI) (Travis et al., 2016), an inability of the model to resolve

vertical mixing in the boundary layer, and a weak response to cloud cover (Travis et al., 2017). Travis et al. (2016)

find that the 3.5 Tg N y^{-1} NEI 2011 estimate for U.S. fuel NOx emissions is too high and contributes to excessive

surface O$_3$. Our simulations include even higher U.S. fuel NOx emissions of 4.4 Tg N y^{-1} during 2010-2012

(Supplemental Table 3), implying that some portion of the model O$_3$bias reflects excessively high anthropogenic

230   NOx emissions (Travis et al., 2016). The low bias in cloud cover in the MERRA meteorology and associated

overestimate in downward shortwave surface radiation (Free et al., 2016) may also contribute to excessive O$_3$

production in the model. The model is closest to the observations in spring, with a positive bias usually <10 ppb

over the eastern states and generally within ±5 ppb over most western sites (Figure 2a, b, c).

3.2 Baseline O$_3$ at Mount Bachelor

235   Mount Bachelor Observatory (MBO) regularly samples free tropospheric O$_3$ and is rarely influenced by

local anthropogenic emissions (Reidmiller et al., 2009). It is therefore, a valuable site for examining baseline O$_3$. In

Supplemental Figure 4, we compare the observed 24-hour and MDA8 O$_3$ concentrations at MBO for 2004-2012.

The observed O$_3$ concentrations vary from year to year, and by definition, MDA8 O$_3$ is a few ppb higher than the

24-hour mean mixing ratios. However, the seasonal pattern is similar across both metrics, with a springtime peak,

240   maximum in April, and a secondary summertime peak in July.

Figure 3 compares modeled and observed monthly mean 24-hour O$_3$ concentrations at the grid box that

contains Mount Bachelor. For the model, we examine O$_3$_Base and O$_3$_USB 24-hour average concentrations at 2.7

km, the height of the Mount Bachelor Observatory, as well as at the surface. It is important to note that the diurnal

variations on the mountain may not be well captured by the CTM, due to upslope (daytime)/downslope (nighttime)

245   flow. We focus on the 24-hour average because we only archived hourly O$_3$ fields from the model at the surface and

thus, do not have the MDA8 O$_3$ metric available at 2.7 km. The year-to-year variability is smaller in the model than

observed (narrower shaded range). In all months, the O$_3$_Base and O$_3$_USB values are higher by 9-14 ppb and 11-21

ppb, respectively, at 2.7 km than at the surface. The model captures the magnitude of the observed springtime peak

at 2.7 km, but summertime values are too high, with an overall peak in August. O$_3$_USB contributes a greater

250   fraction to O$_3$_Base at 2.7 km (92-94%) than at the surface (72-94%). The simulated seasonal cycle differs at the

surface, peaking in spring (March-April) and in September. In 2012, the observations show equivalent springtime

and summertime peaks, more similar to the modeled seasonal cycle. While the observations generally decline from

spring into summer, the model indicates an increase, leading to a substantial model overestimate during summer in most years. This model bias occurs across much of the U.S.A. as we show below.

255   Our sensitivity simulations enable us to interpret the sources contributing to the simulated seasonal distribution. The model indicates that at MBO, O_3_USB is the major component of O_3_Base, including during the summertime overestimate. In turn, the model indicates that the seasonality of O_3_USB is largely driven by O_3_NAT, which includes the influence from biogenic VOC and NOx, lightning NO_x, as well as stratospheric O_3. O_3_ICT+CH_4 contributes around 15 ppb at 2.7km and 5-10 ppb at the surface (Figure 3). The model does suggest a springtime

260   peak influence from O_3_ICT+CH_4 in the WUS, consistent with earlier work (e.g., Task Force on Hemispheric Transport of Air Pollution, 2010). Even at this baseline site, the model indicates that O_3_USA enhances monthly mean O_3 by at least a few ppb at 2.7 km; at the surface, the model simulates a seasonal cycle for O_3_USA that is typical of photochemical production from regional precursor emissions. O_3_CA+MX is less than a few ppb at MBO whether the model is sampled at 2.7 km or the surface (not shown).

265   **3.3 Magnitude and timing of high-O_3 events**

On O_3_top10obs days, the model biases are typically lower than on average days (Figure 2, Table 2; see also year-by-year maps in Supplemental Figure 2). At some WUS sites, the model underestimates O_3 levels during the highest events by 10-20 ppb. The model systematically underestimates O_3 in the Central Valley of California in all three seasons, which we attribute to the inability of the coarse model resolution to resolve topographical gradients

270   and valley circulations (or stagnation) in this region which experiences some of the highest observed O_3 in the nation.

We compare the MDA8 O_3 distributions in the observations versus the model (O_3_Base) during the 10 most biased days in each of the ten regions across the nine years (900 total events). These "most-biased" days in the model tend to fall around the observed median (Figure 1c) during the warm season (June - October), with

275   almost 40% of the days falling in August alone (Supplemental Figure 5), and are 9-45 ppb higher than the observations (circles in Supplemental Figure 6). We analyze the perturbation simulations (Table 1) to identify which sources influence simulated O_3 most strongly on the "most-biased" days versus on average (i.e., all 365 or 366 days), which we assume are also likely the main drivers of the bias. In all regions, the largest sources on the "most-biased" model days are O_3_USA (3-30 ppb higher MDA8 O_3 than on average with the exception of the

280   Pacific SW where O$_3$_USA is smaller than on average days), O$_3$_BVOC (by 1-15 ppb), and O$_3$_SNO$_x$ (by 1-10

ppb; Figure 4, Supplemental Figure 6). By contrast, O$_3$_ICT+CH$_4$ is up to a few ppb higher on average days than

on the most-biased model days.

To explore possible drivers of model biases across the different seasons, we evaluate the timing of the

highest ten events across each year in the O$_3$_Base, O$_3$_USB, and O$_3$_noBVOC (BVOCs shut off) simulations for

285   each region (900 events). We bin these 900 events by month and calculate the percentage of the total events that

fall within each month. Note that all the top ten days fall between March and October. The standard model

(O$_3$_Base) underestimates the occurrence of high events early in the O$_3$ season (March-June) and overestimates

them later in the season (July-September) (Supplemental Figure 7). While the model indicates that most top ten O$_3$

days fall between July-August (35% each), the observations show that May through August each contain around

290   15-25% with the maximum in June at 25%. Both O$_3$_noBVOC and O$_3$_USB shift the relative timing of the 10

highest O$_3$ events towards April and May compared to O$_3$_Base, but the shortage of high springtime O$_3$ events

remains (Supplemental Figure 7). The lack of high events in spring may reflect in part poor representation of

stratospheric O$_3$ intrusions at the coarse resolution of the CTM (Lin et al., 2012; Zhang et al., 2014), in addition to

the role of U.S. anthropogenic and BVOC emissions in the temporal mis-match as indicated by the improvements

295   to the timing that occur in the O$_3$_USB (U.S. anthropogenic emissions shut off) and O$_3$_noBVOC simulations. In

addition to contributions from these sources, poor representation of O$_3$ sinks may contribute to the model biases.

For example, Makar et al. (2017) suggest that failing to represent canopy turbulence and shading effects on

photolysis can lead to high-O$_3$ biases in models.

3.4 Interannual variability

300   Supplemental Figure 8 shows the Pearson correlations coefficients (r) between monthly average observed

and O$_3$_Base values from 2004-2012. In May, correlations are generally strong ($r \geq 0.9$) in the Mid-Atlantic and

Southeast regions, but much lower ($r = 0.2$) in the New England region. This pattern may reflect shortcomings in

representing the onset of BVOC emissions. In July, the regions flip, with lower correlations in the Southeast and

higher correlations in New England. At some sites in the WUS, lower correlations occur during summer months,

305   which may be tied to excessive influence from lightning NO$_x$ advected from Mexico (see also Zhang et al., 2011;

2014) or anomalous events such as wildfires that are not well captured by the model.

In general, correlations only average about $r = 0.2$ in the winter and early spring over much of the United States (Supplemental Figure 8); the drivers for these weak correlations may be connected to the model tendency to underestimate the occurrence of springtime high-O_3 events. From May to September, however, the months during which high-O_3 events are most likely to occur, the correlation between 2004-2012 observed and simulated O_3 monthly averages over much of the contiguous United States exceed $r = 0.7$ (Supplemental Figure 8). We conclude that the model broadly captures monthly variations from year-to-year during the warm season and can thus be applied to interpret the role of background sources in contributing to interannual variations during most of the high-O_3 season. We note that Clifton et al. (2017) found that the GEOS-Chem model does not capture interannual variability in deposition velocities observed at Harvard Forest, MA, but it is unclear to what extent this process would amplify or dampen interannual variability associated with changes in emissions.

4   Influence of individual sources on average versus high-O_3 days

In Table 2 and Table 3, we report the influence of the O_3 sources defined in Table 1 on average versus $O_3\_top10obs$ days separately for spring (MAM), summer (JJA), and fall (SON) (ten days from each of the nine simulation years for 900 events for each region and season). We also report the difference in source influences between average and $O_3\_top10obs$ days, which we interpret as the enhancement from that source relative to average conditions.

We first consider the average ranges in MDA8 O_3 contributed by the various sources. Both O_3_USA and O_3_USB tend to follow the seasonal cycle of O_3_Base, with highest abundances in summer. The model indicates that O_3_USB is 30-50 ppb (range over regions) during summer and highest over the WUS. O_3_USA is generally 20-30 ppb over the EUS in summer, but only 10-20 ppb over the WUS (Table 2). $O_3\_ICT+CH_4$ averages 2-13 ppb over all regions and is highest in spring (8-13 ppb compared to 2-11 ppb in summer and 6-12 ppb in fall) (Table 3, Figure 5, Supplemental Figure 9). $O_3\_NALNO_x$ has a relatively minor influence (at most 1.5 ppb) in all regions and seasons. The influence from O_3_CA+MX is generally less than a couple of ppb except in NY+NJ and New England where it can be as much as 4-7 ppb (Table 3, Supplemental Figure 9).

We interpret the "difference" lines in Table 2 and Table 3 as the enhancements from each source on high days in each season ($O_3\_top10obs\_MAM$, $O_3\_top10obs\_JJA$, $O_3\_top10obs\_SON$) relative to average conditions. Over all regions, O_3_BVOC and $O_3\_SNO_x$ influence O_3_Base more on $O_3\_top10obs$ days (for all seasons) than on

average whereas $O_3\_ICT+CH_4$ is typically lower by up to 3 ppb on $O_3\_top10obs$ days (for all seasons) than on

335   average days (Table 2, Table 3, Figure 5, Supplemental Figure 9). O_3_USA is 8-11 ppb higher on $O_3\_top10obs\_JJA$

days versus average over the New England, NY+NJ, Mid-Atlantic, Midwest, and South Central regions, but only up

to 5 ppb higher over other regions (Table 2, Figure 5, Supplemental Figure 9). The model indicates an even stronger

anthropogenic enhancement (up to 19 ppb) on $O_3\_top10obs\_SON$ days in some EUS regions (Table 2). O_3_USB is

enhanced on $O_3\_top10obs\_JJA$ days by 2-12 ppb relative to average, with the smallest enhancements occurring in

340   the Mid-Atlantic, Southeast, and Midwest regions, and the largest enhancements occurring in the Pacific NW. In

contrast to all the other regions, O_3_USB is the dominant source enhancing $O_3\_top10days\_JJA$ over the Mountains

and Plains, Pacific NW, and Pacific SW regions (4-12 ppb for O_3_USB but < 5 ppb from either O_3_USA or

O_3_BVOC). In line with earlier work reviewed by Jaffe et al. (2017), enhanced O_3_USA dominates

$O_3\_top10obs\_JJA$ days over much of the U.S.A., whereas in the WUS, O_3_USB enhancements exceed O_3_USA

345   enhancements on $O_3\_top10days\_JJA$. O_3_BVOC enhances $O_3\_top10obs$ days (for all seasons) by up to 9 ppb, with

the influence often largest in fall (when O_3 formation is more sensitive to VOC; e.g., Jacob et al., 1995). We re-

emphasize that BVOCs contribute both to O_3_USA when reacting with anthropogenic NO_x and to O_3_USB when

reacting with all other NO_x sources. In contrast to the sources discussed above, $O_3\_ICT+CH_4$ influences average

days by up to a few ppb more than on $O_3\_top10obs$ days (for all seasons), with the largest differences between

350   average and high days occurring in EUS regions (1-3 ppb lower on $O_3\_top10obs$ days (for all seasons) in New

England, NY+NJ, Mid-Atlantic; Table 3, Figure 5, Supplemental Figure 9). $O_3\_NALNO_x$ is at most 2 ppb higher

than average on $O_3\_top10obs$ days. The O_3_CA+MX influence is roughly equivalent (generally to within a ppb) on

average versus $O_3\_top10obs$ days during all seasons.

5   Interannual variability in the sources influencing high vs. average ground-level O_3

355   Despite its high mean bias and seasonal phase shift, the model does capture some of the observed

interannual variability in observed $O_3\_top10obs\_JJA$ MDA8 O_3 concentrations (Figure 6, Supplemental Figure 10; *r*

= 0.5 to ≥ 0.9). Comparing the 2004-2006 period with 2010-2012, both observed and simulated MDA8 O_3

concentrations on $O_3\_top10obs\_JJA$ days hold steady or decrease across all regions. This change reflects opposing

influences in the model: rising O_3_USB (by 2 ppb averaged over all regions) and declining O_3_USA concentrations

360   (by 6 ppb averaged over all regions) (Figure 6, Table 4, Supplemental Figure 10). We note that over the Pacific NW

there is a 4 ppb decrease in O_3_USB from 2004-2006 to 2010-2012. Over this period, temperatures generally warm over the EUS, but slightly cool in the WUS. Within the ten regions, the model captures the sign of the changes in MDA8 O_3 over this period but not the magnitude (Table 4). The model monthly mean temperatures in the model (from the MERRA reanalysis) closely match the observed GHCN+CAMS dataset (Supplemental Table 4). Table 4

365   shows that regions with O_3_USB increases generally experienced rising temperatures over this period, as the 2010-2012 period includes two of the warmest years on record. Figure 6 shows that O_3_NAT tracks with O_3_USB and temperature (dips in MDA8 O_3 occur during years with cooler temperatures (2008-2009) and increases in years with warmer temperatures (2011-2012), indicating that year-to-year variability in O_3_USB on O_3_top10obs_JJA days is primarily driven in the model by natural sources sensitive to meteorology rather than international O_3 transport

370   (Figure 6, Supplemental Figure 10). Although 2012 was the hottest year on average between 2004-2012 (except in the Pacific NW where 2004 was warmer by about a degree), it was not the hottest summer in all regions.

We find that O_3_USB drives the interannual variability on O_3_top10obs_JJA days in the WUS ($r = 0.72$-0.85 for O_3_USB versus O_3_Base, whereas $r = 0.05$-0.64 for O_3_USA versus O_3_Base; Supplemental Table 5). In NY+NJ, the Southeast, Midwest, South Central, and Plains regions, O_3_USB and O_3_USA both contribute to the

375   interannual variability on O_3_top10obs_JJA days ($r = 0.5$-0.8 for both O_3_USB and O_3_USA versus O_3_Base) while in New England and the Mid-Atlantic regions, O_3_USA drives the interannual variability more than O_3_USB ($r = 0.64$ and 0.72 for O_3_USA versus O_3_Base but only 0.28 and 0.54, respectively, for O_3_USB versus O_3_Base; Supplemental Table 5).

Year-to-year variations in monthly average O_3_USB are relatively large, with 10-15 ppb differences

380   between the highest and lowest O_3_USB years during the warmest months (Figure 7, Supplemental Figure 11). Seasonal variations also differ by region, especially during summer. For example, the western U.S. regions have a smooth seasonal cycle with O_3_USB concentrations rising from January to a peak in July and August, and then declining again. Interannual and seasonal variability in O_3_USB are generally greater in the Southeast than in the Mountains and Plains, and Plains regions (Figure 7, Supplemental Figure 11). Year-to-year variability in O_3_BVOC

385   is smaller than O_3_USB, with a maximum range of about 10 ppb between the highest and lowest years during August (Figure 7, Supplemental Figure 12). O_3_SNOx ranges by a few ppb throughout the summer in the Southeast, and by up to 6 ppb over the Mountains and Plains in August (Figure 7, Supplemental Figure 13).

O$_3$_USA anomalies relative to the 2004-2012 average illustrate declining influence in all regions, with negative anomalies after 2007 on both O$_3$_top10obs and average days (Figure 8, Supplemental Figure 14). This finding is well established by earlier work demonstrating decreases in high-O$_3$ concentrations as a result of regional NO$_x$ emissions reductions over the past few decades (Cooper et al., 2012, 2014a; Jaffe et al., 2018; Young et al., 2017). O$_3$_BVOC is the main driver of the high and low O$_3$ anomalies (up to ±5 ppb on O$_3$_top10obs_JJA days) from year-to-year (Figure 8, Supplemental Figure 15).

Specific events can affect O$_3$ in any given year. For example, in 2008, there were extensive fires across much of California in May, June, and July. In 2008, the Pacific SW region that includes California, Nevada, and Arizona, shows a positive anomaly in O$_3$_BB (> 1 ppb) on the O$_3$_top10obs days, stronger than during any other year in that region (Supplemental Figure 15). If we restrict our analysis solely to Reno, NV, the anomaly for O$_3$_BB was 7 ppb in July 2008 relative to the 2004-2012 July average (not shown). We emphasize that a single location can be more strongly influenced by a specific source than the regional averages on which we have focused.

Currently, the U.S. EPA uses a 3-year averaging period of the 4th-highest MDA8 O$_3$ to assess compliance with the O$_3$ NAAQS. We evaluate the extent to which this 3-year averaging period removes interannual variability in meteorology (the grounds for the averaging) (Figure 9, Supplemental Figure 16). The observed range is generally much smaller than the model estimate. We find that the 3-year average of the 4th highest day decreases the range by 2-6 ppb and 5-18 ppb in the observations and O$_3$_Base respectively when compared to taking the 4th highest day in any given year when we look across all regions (Table 5). However, the 3-year average of the 4th highest day still ranges from 3-9 ppb and 2-11 ppb in the observations and O$_3$_Base, respectively, across all regions (compared to 5-15 ppb and 10-36 ppb in the observations and O$_3$_Base on the 4th highest day in each individual year). Thus, while averaging across the years decreases the spread, variability remains. In keeping with our previous analysis of the O$_3$_top10obs days, we compare the spread of the 4th highest O$_3$ day in each of the three years to the range of the O$_3$_top10obs days across each three year span; the 4th highest days can range almost as widely as the O$_3$_top10obs days in some years, but in other years, are clustered closer together (Figure 9). Figure 9 shows that the range in O$_3$_top10obs days for O$_3$_Base generally correlates with O$_3$_UBS in the WUS, suggesting that O$_3$_USB is the dominant influence on the high days there, but there is little correlation in the EUS. We

conclude that a three-year smoothing period is not long enough to eliminate entirely the interannual variability in

415   MDA8 O_3 levels, and in the WUS, this interannual variability tends to reflect variations in O3_USB.

6   Discussion and Conclusions

As air quality controls decrease U.S. anthropogenic precursor emissions to O_3, the relative importance of the

background influence on total surface O_3 increases. We use O_3 MDA8 concentrations spanning 2004-2012 from the

EPA AQS, CASTNet, and Mount Bachelor Observatory sites, and sensitivity simulations from the global GEOS-

420   Chem 3D chemistry transport model to estimate the influence from various individual background sources on O_3 in

each of the ten EPA regions in the continental U.S.A. The global scale of the GEOS-Chem model allows us to quantify

intercontinental transport (including global methane) in addition to regional natural and anthropogenic sources of O_3.

The sensitivity simulations span nine years, allowing us to examine the role of these sources in contributing to

interannual variability. Our analysis contrasts average- and high-O_3 days.

425   Correlations between monthly averages across 2004-2012 show that the model captures monthly variations

from year-to-year, especially during summer (JJA). The model shows substantial variability in simulated U.S.

background O_3 concentrations from year-to-year, on the order of 10-20 ppb between 2004-2012 in summer (Figure

7). We find that the extent to which the current three-year averaging period for assessing compliance with the National

Ambient Air Quality Standard for O_3 succeeds in smoothing out interannual variability depends on the range in

430   consecutive years, and thus varies by region and time period, but is generally not long enough to completely eliminate

the interannual variability in background O_3 (Figure 9).

We find substantial biases in the severity (+0-19 ppb in maximum daily 8-hour average (MDA8) O_3) and

timing of high-O_3 events in the model. The model underestimates the frequency of high events in spring, possibly

associated with stratospheric intrusions (Fiore et al., 2014; Zhang et al., 2011; 2014). Future efforts would benefit

435   from quantifying the stratospheric (as well as Asian) influence alongside the other background sources we consider.

We find a stronger influence of U.S. anthropogenic emissions on regionally averaged MDA8 O_3 (up to 30 ppb) from

BVOCs (up to 15 ppb) and soil NO_x (up to 10 ppb) on the ten most biased days as compared to average days. We

conclude that regional production of O_3 is driving the pervasive high positive model bias in summer, as opposed to

transported background, although our sensitivity simulations do not allow us to rule out the possibility of a

440   coincident missing sink.

Our finding that BVOC emissions contribute to the summertime surface O_3 biases could reflect poor representation of the emissions (and subsequent oxidation chemistry). Earlier work has noted that MEGAN BVOC emissions are too high over California (Bash et al., 2016), Southeast Texas (Kota et al., 2015), the Ozarks in southern Missouri (Carlton and Baker, 2011), and across much of the U.S.A. (Wang et al., 2017). One recent model

445   study uniformly reduced MEGAN isoprene emissions by 20% (Li et al., ACP 2018), but we did not apply any such scaling here. In regions that are highly NOx-sensitive, additional isoprene should not strongly influence O_3, as found over southeast Texas (Kota et al., 2015). While not eliminated entirely, the summertime model bias does lessen in the simulation with BVOC emissions set to zero, suggesting that the O_3 bias is indeed exacerbated if BVOC emissions are overestimated in the model.

450   On the ten days with the highest observed MDA8 O_3 values (O_3_top10obs) in each season, the model indicates that U.S. anthropogenic and biogenic VOC emissions are the most important drivers relative to average days, over most regions (Table 2, Table 3). O_3_top10obs_MAM and O_3_top10obs_SON days (i.e., the ten highest spring and fall MDA8 O_3 days) are up to 9°C warmer than average, but O_3_top10obs_JJA days (i.e., the ten highest summer MDA8 O_3 days) are only 1-2 °C warmer than average (Table 2). U.S. anthropogenic emissions enhance

455   O_3_top10obs_JJA days by 5-11 ppb above average in the eastern U.S. regions, but by less than 2 ppb over the three western regions. Over these westernmost regions, U.S. background O_3 is 4-12 ppb higher on O_3_top10obs_JJA days than on average (Table 2). Across the continental U.S.A., biogenic VOC emissions enhance O_3 by 1-7 ppb above average on O_3_top10obs_JJA days, while intercontinental pollution is either similar or up to 2 ppb higher on average days (Table 3). Analysis of our simulations thus indicates that the highest O_3 events are associated with regional O_3

460   production rather than transported background.

From 2004-2006 to 2010-2012, MDA8 O_3 concentrations on O_3_top10obs_JJA days vary from year-to-year, but show little overall trend, decreasing by 3 ppb in both the observations and the model averaged over all regions (Figure 6, Table 4). With our sensitivity simulations, we interpret this lack of an overall trend as a balance between rising U.S. background O_3 (by 2 ppb for O_3_USB from 2004-2006 to 2010-2012 averaged over all regions) and

465   declining U.S. anthropogenic emissions (by 6 ppb for O_3_USA from 2004-2006 to 2010-2012 averaged over all regions). The declining influence of U.S. anthropogenic emissions on O_3_top10obs_JJA days is consistent with earlier

work showing high-O_3 concentrations decreasing in response to regional precursor emissions controls since the late 1990s (e.g. Cooper et al., 2012, 2014b; Frost et al., 2006; Simon et al., 2016).

470   In contrast to previous work, including with the GEOS-Chem model (e.g. Fiore et al., 2014 and references therein), we find that U.S. background O_3 tends to be higher in summer than in spring in most regions. This likely reflects differences in the isoprene chemistry, specifically the isoprene nitrates, between our version of GEOS-Chem (Mao et al., 2013) and older versions that treat isoprene nitrates as greater sinks for NO_x and thereby, suppress O_3 production. The coarse resolution of our model will excessively mix isoprene and soil NO_x sources (e.g., Yu et al., 2016), and thus may exaggerate the relative importance of enhanced background O_3 resulting from soil NO_x and

475 isoprene. Nevertheless, the model skill at capturing the observed year-to-year variability in the regionally averaged ten highest days lends some confidence to its attribution of this variability to natural sources (e.g. Figure 6). Future work with high-resolution models (e.g., at the regional scale, ideally with boundary conditions that include source attributions from a global model) is needed, along with observational evidence, to quantify the extent to which biogenic VOC and NO_x contribute to the highest observed O_3 levels in the warm season. The importance of

480 temperature sensitive sources like biogenic VOC and NO_x emissions to background O_3 imply that in a warmer climate, these background influences on O_3 will play an even more important role in driving up O_3 levels.

Acknowledgments

      We acknowledge insightful discussions with Gail Tonnesen and Pat Dolwick (U.S. EPA). We gratefully acknowledge support from NASA AQAST (NNX12AF15G) and NASA HAQAST (NNX16AQ20G). This project

485 has been funded in part by the United States Environmental Protection Agency under assistance agreement RD83587801 to AMF. The contents of this document do not necessarily reflect the views and policies of the Environmental Protection Agency, nor does the EPA endorse trade names or recommend the use of commercial products mentioned in this document. Upon publication, data behind the figures will be provided online at Columbia University Academic Commons.

490   **References**

Abatzoglou, J. T. and Williams, A. P.: Impact of anthropogenic climate change on wildfire across western US forests, Proc. Natl. Acad. Sci., 113(42), 11770–11775, doi:10.1073/pnas.1607171113, 2016.

Auvray, M. and Bey, I.: Long-range transport to Europe: Seasonal variations and implications for the European ozone budget, J. Geophys. Res., 110(D11), D11303, doi:10.1029/2004JD005503, 2005.

495   Barkley, M. P., Palmer, P. I., Ganzeveld, L., Arneth, A., Hagberg, D., Karl, T., Guenther, A., Paulot, F., Wennberg, P. O., Mao, J., Kurosu, T. P., Chance, K., Müller, J. F., De Smedt, I., Van Roozendael, M., Chen, D., Wang, Y. and Yantosca, R. M.: Can a "state of the art" chemistry transport model simulate Amazonian tropospheric chemistry?, J. Geophys. Res. Atmos., 116(16), D16302, doi:10.1029/2011JD015893, 2011.

Baylon, P. M., Jaffe, D. A., Pierce, R. B. and Gustin, M. S.: Interannual Variability in Baseline Ozone and Its
500   Relationship to Surface Ozone in the Western U.S., Environ. Sci. Technol., 50(6), 2994–3001, doi:10.1021/acs.est.6b00219, 2016.

Bond, T. C., Bhardwaj, E., Dong, R., Jogani, R., Jung, S., Roden, C., Streets, D. G. and Trautmann, N. M.: Historical emissions of black and organic carbon aerosol from energy-related combustion, 1850-2000, Global Biogeochem. Cycles, 21(2), 1850–2000, doi:10.1029/2006GB002840, 2007.

505   Bosilovich, M. G.: Regional climate and variability of NASA MERRA and recent reanalyses: U.S. summertime precipitation and temperature, J. Appl. Meteorol. Climatol., 52(8), 1939–1951, doi:10.1175/JAMC-D-12-0291.1, 2013.

Bouwman, A. F., Lee, D. S., Asman, W. A. H., Dentener, F. J., Van Der Hoek, K. W. and Olivier, J. G. J.: A global high-resolution emission inventory for ammonia, Global Biogeochem. Cycles, 11(4), 561–587,
510   doi:10.1029/97GB02266, 1997.

Clifton, O. E., Fiore, A. M., Munger, J. W., Malyshev, S., Horowitz, L. W., Shevliakova, E., Paulot, F., Murray, L. T. and Griffin, K. L.: Interannual variability in ozone removal by a temperate deciduous forest, Geophys. Res. Lett., 44(1), 542–552, doi:10.1002/2016GL070923, 2017.

Cooper, O. R., Gao, R.-S., Tarasick, D., Leblanc, T. and Sweeney, C.: Long-term ozone trends at rural ozone
515   monitoring sites across the United States, 1990-2010, J. Geophys. Res. Atmos., 117(22), n/a-n/a, doi:http://dx.doi.org/10.1029/2012JD018261, 2012.

Cooper, O. R., Parrish, D. D., Ziemke, J., Balashov, N. V., Cupeiro, M., Galbally, I. E., Gilge, S., Horowitz, L., Jensen, N. R., Lamarque, J.-F., Naik, V., Oltmans, S. J., Schwab, J., Shindell, D. T., Thompson, A. M., Thouret, V., Wang, Y. and Zbinden, R. M.: Global distribution and trends of tropospheric ozone: An observation-based review,
520   Elem. Sci. Anthr., 2, 29, doi:10.12952/journal.elementa.000029, 2014a.

Cooper, O. R., Parrish, D. D., Ziemke, J., Balashov, N. V., Cupeiro, M., Galbally, I. E., Gilge, S., Horowitz, L., Jensen, N. R., Lamarque, J.-F., Naik, V., Oltmans, S. J., Schwab, J., Shindell, D. T., Thompson, A. M., Thouret, V., Wang, Y. and Zbinden, R. M.: Global distribution and trends of tropospheric ozone: An observation-based review, Elem. Sci. Anthr., 2(0), 29, doi:10.12952/journal.elementa.000029, 2014b.

525   van Donkelaar, A., Martin, R. V, Leaitch, W. R., Macdonald, A. M., Walker, T. W., Streets, D. G., Zhang, Q., Dunlea, E. J., Jimenez, J. L., Dibb, J. E., Huey, L. G., Weber, R. and Andreae, M. O.: Analysis of aircraft and satellite measurements from the Intercontinental Chemical Transport Experiment (INTEX-B) to quantify long-range transport of East Asian sulfur to Canada, Atmos. Chem. Phys. Atmos. Chem. Phys., 8, 2999–3014 [online] Available from: www.atmos-chem-phys.net/8/2999/2008/ (Accessed 23 August 2016), 2008.

530   Fan, Y. and van den Dool, H.: A global monthly land surface air temperature analysis for 1948-present, J. Geophys. Res., 113(D1), 18, doi:10.1029/2007jd008470, 2008.

Fiore, A. M., Jacob, D. J., Field, B. D., Streets, D. G., Fernandes, S. D. and Jang, C.: Linking ozone pollution and climate change: The case for controlling methane, Geophys. Res. Lett., 29(19), 1919, doi:10.1029/2002GL015601, 2002.

535   Fiore, A. M., Jacob, D. J., Liu, H., Yantosca, R. M., Fairlie, T. D. and Li, Q.: Variability in surface ozone background over the United States: Implications for air quality policy, J. Geophys. Res., 108(D24), 4787, doi:10.1029/2003jd003855, doi:10.1029/2003jd003855, 2003.

Fiore, A. M., Oberman, J. T., Lin, M., Zhang, L., Clifton, O. E., Jacob, D. J., Naik, V., Horowitz, L. W., Pinto, J. P. and Milly, G. P.: Estimating North American background ozone in U.S. surface air with two independent global
540   models: Variability, uncertainties, and recommendations, Atmos. Environ., 96, 284–300, doi:10.1016/j.atmosenv.2014.07.045, 2014.

Fiore, A. M., Vaishali, N. and Leibensperger, E. M.: Air Quality and Climate Connections, J. Air Waste Manage. Assoc., 2015.

Free, M., Sun, B. and Yoo, H. L.: Comparison between total cloud cover in four reanalysis products and cloud

545   measured by visual observations at U.S. weather stations, J. Clim., 29(6), 2015–2021, doi:10.1175/JCLI-D-15-0637.1, 2016.

Frost, G. J., McKeen, S. A., Trainer, M., Ryerson, T. B., Neuman, J. A., Roberts, J. M., Swanson, A., Holloway, J. S., Sueper, D. T., Fortin, T., Parrish, D. D., Fehsenfeld, F. C., Flocke, F., Peckham, S. E., Grell, G. A., Kowal, D., Cartwright, J., Auerbach, N. and Habermann, T.: Effects of changing power plant NOx emissions on ozone in the

550   eastern United States: Proof of concept, J. Geophys. Res., 111(D12), D12306, doi:10.1029/2005JD006354, 2006.

Giglio, L., Randerson, J. T., Van Der Werf, G. R., Kasibhatla, P. S., Collatz, G. J., Morton, D. C. and Defries, R. S.: Assessing variability and long-term trends in burned area by merging multiple satellite fire products, Biogeosciences, 7(3), 1171–1186, doi:10.5194/bg-7-1171-2010, 2010.

Guenther, A. B., Jiang, X., Heald, C. L., Sakulyanontvittaya, T., Duhl, T., Emmons, L. K. and Wang, X.: The model

555   of emissions of gases and aerosols from nature version 2.1 (MEGAN2.1): An extended and updated framework for modeling biogenic emissions, Geosci. Model Dev., 5(6), 1471–1492, doi:10.5194/gmd-5-1471-2012, 2012.

Hu, L., Millet, D. B., Baasandorj, M., Griffis, T. J., Travis, K. R., Tessum, C. W., Marshall, J. D., Reinhart, W. F., Mikoviny, T., Müller, M., Wisthaler, A., Graus, M., Warneke, C. and de Gouw, J.: Emissions of C_6 -C_8 aromatic compounds in the United States: Constraints from tall tower and aircraft measurements, J. Geophys. Res. Atmos.,

560   120(2), 826–842, doi:10.1002/2014JD022627, 2015.

Jacob, D. J., Horowitz, L. W., Munger, J. W., Heikes, B. G., Dickerson, R. R., Artz, R. S. and Keene, W. C.: Seasonal transition from NO\~ x-to hydrocarbon-limited conditions for ozone production over the eastern United States in September, J. Geophys. Res., 100, 9315–9315, doi:10.1029/94JD03125, 1995.

Jaffe, D. A.: Relationship between surface and free tropospheric ozone in the Western U.S., Environ. Sci. Technol.,

565   45(2), 432–8, doi:10.1021/es1028102, 2011.

Jaffe, D. A., Cooper, O. R., Fiore, A. M., Henderson, B. H., Gail, S., Russell, A. G., Henze, D. K., Langford, A. O., Lin, M. and Moore, T.: Scientific assessment of background ozone over the U.S.: implications for air quality management, [online] Available from: file:///C:/Users/shizi/Downloads/BOSA_complete_v6.pdf, 2018.

Kuhns, H. and Green, M.: Big Bend Regional Aerosol and Visibility Observational (BRAVO) Study Emissions

570   Inventory, Desert Res. …, 89119(702) [online] Available from: http://citeseerx.ist.psu.edu/viewdoc/download?doi=10.1.1.462.8648&rep=rep1&type=pdf (Accessed 29 January 2018), 2003.

Lee, C., Martin, R. V., van Donkelaar, A., Lee, H., Dickerson, R. R., Hains, J. C., Krotkov, N., Richter, A., Vinnikov, K. and Schwab, J. J.: SO$_2$ emissions and lifetimes: Estimates from inverse modeling using in situ and

575   global, space-based (SCIAMACHY and OMI) observations, J. Geophys. Res., 116(D6), D06304, doi:10.1029/2010JD014758, 2011.

Leibensperger, E. M., Mickley, L. J., Jacob, D. J., Chen, W.-T., Seinfeld, J. H., Nenes, A., Adams, P. J., Streets, D. G., Kumar, N. and Rind, D.: Climatic effects of 1950–2050 changes in US anthropogenic aerosols – Part 2: Climate response, Atmos. Chem. Phys., 12(7), 3349–3362, doi:10.5194/acp-12-3349-2012, 2012.

580   Lin, M., Fiore, A. M., Cooper, O. R., Horowitz, L. W., Langford, A. O., Levy, H., Johnson, B. J., Naik, V., Oltmans, S. J. and Senff, C. J.: Springtime high surface ozone events over the western United States: Quantifying the role of stratospheric intrusions, J. Geophys. Res. Atmos., 117(D21), doi:10.1029/2012JD018151, 2012.

Lin, M., Fiore, A. M., Horowitz, L. W., Langford, A. O., Oltmans, S. J., Tarasick, D. and Rieder, H. E.: Climate variability modulates western US ozone air quality in spring via deep stratospheric intrusions., Nat. Commun.,

585   6(May), 7105, doi:10.1038/ncomms8105, 2015a.

Lin, M., Horowitz, L. W., Cooper, O. R., Tarasick, D., Conley, S., Iraci, L. T., Johnson, B. J., Leblanc, T., Petropavlovskikh, I. and Yates, E. L.: Revisiting the evidence of increasing springtime ozone mixing ratios in the free troposphere over western North America, Geophys. Res. Lett., 42(20), 8719–8728, doi:10.1002/2015GL065311, 2015b.

590   Lin, M., Horowitz, L. W., Payton, R., Fiore, A. M. and Tonnesen, G.: US surface ozone trends and extremes from 1980-2014: Quantifying the roles of rising Asian emissions, domestic controls, wildfires, and climate, Atmos. Chem. Phys. Discuss., 1–56, doi:10.5194/acp-2016-1093, 2016.

Mao, J., Horowitz, L. W., Naik, V., Fan, S., Liu, J. and Fiore, A. M.: Sensitivity of tropospheric oxidants to biomass burning emissions: implications for radiative forcing, Geophys. Res. Lett., 40(6), 1241–1246,

595   doi:10.1002/grl.50210, 2013.

National Research Council: Global Sources of Local Pollution: An Assessment of Long-Range Transport of Key Air Pollutants to and from the United States, The National Academies Press, Washington, DC., 2010.

Olivier, J. G. J., Van Aardenne, J. A., Dentener, F. J., Pagliari, V., Ganzeveld, L. N. and Peters, J. A. H. W.: Recent trends in global greenhouse gas emissions:regional trends 1970–2000 and spatial distributionof key sources in 2000,

600   Environ. Sci., 2(2–3), 81–99, doi:10.1080/15693430500400345, 2005.

Reidmiller, D. R., Fiore, A. M., Jaffe, D. A., Bergmann, D., Cuvelier, C., Dentener, F. J., Duncan, B. N., Folberth, G. A., Gauss, M., Gong, S., Hess, P., Jonson, J. E., Keating, T., Lupu, A., Marmer, E., Park, R. J., Schultz, M. G., Shindell, D. T., Szopa, S., Vivanco, M. G., Wild, O. and Zuber, A.: The influence of foreign vs. North American emissions on surface ozone in the US, Atmos. Chem. Phys., 9(14), 5027–5042, doi:10.5194/acp-9-5027-2009, 2009.

605   Rienecker, M. M., Suarez, M. J., Gelaro, R., Todling, R., Bacmeister, J., Liu, E., Bosilovich, M. G., Schubert, S. D., Takacs, L., Kim, G. K., Bloom, S., Chen, J., Collins, D., Conaty, A., Da Silva, A., Gu, W., Joiner, J., Koster, R. D., Lucchesi, R., Molod, A., Owens, T., Pawson, S., Pegion, P., Redder, C. R., Reichle, R., Robertson, F. R., Ruddick, A. G., Sienkiewicz, M. and Woollen, J.: MERRA: NASA's modern-era retrospective analysis for research and applications, J. Clim., 24(14), 3624–3648, doi:10.1175/JCLI-D-11-00015.1, 2011.

610   Schnell, J. L. and Prather, M. J.: Co-occurrence of extremes in surface ozone, particulate matter, and temperature over eastern North America., Proc. Natl. Acad. Sci. U. S. A., 114(11), 2854–2859, doi:10.1073/pnas.1614453114, 2017.

Schnell, J. L., Holmes, C. D., Jangam, A. and Prather, M. J.: Skill in forecasting extreme ozone pollution episodes with a global atmospheric chemistry model, Atmos. Chem. Phys., 14(15), 7721–7739, doi:10.5194/acp-14-7721-

615   2014, 2014.

Schultz, M. G.: REanalysis of the TROpospheric chemical composition over the past 40 years, Reports Earth Syst. Sci., 48 [online] Available from: http://pubman.mpdl.mpg.de/pubman/item/escidoc:994467/component/escidoc:994466/WEB_BzE_48.pdf (Accessed 29 January 2018), 2007.

620   Simon, H., Wells, B., Baker, K. R. and Hubbell, B.: Assessing temporal and spatial patterns of observed and predicted ozone in multiple urban areas, Environ. Health Perspect., 124(9), 1443–1452, doi:10.1289/EHP190, 2016.

Stauffer, R. M., Thompson, A. M., Oltmans, S. J. and Johnson, B. J.: Tropospheric ozonesonde profiles at long-term U.S. monitoring sites: 2. Links between Trinidad Head, CA, profile clusters and inland surface ozone measurements, J. Geophys. Res. Atmos., 122(2), 1261–1280, doi:10.1002/2016JD025254, 2017.

625   Stettler, M. E. J., Eastham, S. and Barrett, S. R. H.: Air quality and public health impacts of UK airports. Part I: Emissions, Atmos. Environ., 45, 5415–5424, doi:10.1016/j.atmosenv.2011.07.012, 2011.

Streets, D. G., Zhang, Q., Wang, L., He, K., Hao, J., Wu, Y., Tang, Y. and Carmichael, G. R.: Revisiting China's CO emissions after the Transport and Chemical Evolution over the Pacific (TRACE-P) mission: Synthesis of inventories, atmospheric modeling, and observations, J. Geophys. Res. Atmos., 111(14), D14306,

630   doi:10.1029/2006JD007118, 2006.

Task Force on Hemispheric Transport of Air Pollution: HEMISPHERIC TRANSPORT OF AIR POLLUTION, Econ. Comm. Eur. [online] Available from: http://www.htap.org/publications/2010_report/2010_Final_Report/HTAP 2010 Part A 110407.pdf (Accessed 30 June 2017), 2010.

635   Travis, K. R., Jacob, D. J., Fisher, J. A., Kim, P. S., Marais, E. A., Zhu, L., Yu, K., Miller, C. C., Yantosca, R. M., Sulprizio, M. P., Thompson, A. M., Wennberg, P. O., Crounse, J. D., St Clair, J. M., Cohen, R. C., Laughner, J. L., Dibb, J. E., Hall, S. R., Ullmann, K., Wolfe, G. M., Pollack, I. B., Peischl, J., Neuman, J. A. and Zhou, X.: Why do models overestimate surface ozone in the Southeast United States?, Atmos. Chem. Phys., 16(21), 13561–13577, doi:10.5194/acp-16-13561-2016, 2016.

640   Travis, K. R., Jacob, D. J., Keller, C. A., Kuang, S., Lin, J., Newchurch, M. J. and Thompson, A. M.: Resolving ozone vertical gradients in air quality models, Atmos. Chem. Phys. Discuss., 1–18, doi:10.5194/acp-2017-596, 2017.

U.S. Environmental Protection Agency: Map of EPA Regions, [online] Available from: http://www.epa.gov/oust/regions/regmap.htm (Accessed 2 December 2015), 2012.

U.S. Environmental Protection Agency: AirData - Download Data. [online] Available from:

645   http://aqsdr1.epa.gov/aqsweb/aqstmp/airdata/download_files.html#Daily, 2014.

Wang, C., Corbett, J. J. and Firestone, J.: Improving spatial representation of global ship emissions inventories, Environ. Sci. Technol., 42(1), 193–199, doi:10.1021/es0700799, 2008.

Wang, H., Jacob, D. J., Le Sager, P., Streets, D. G., Park, R. J., Gilliland, A. B. and van Donkelaar, A.: Surface ozone background in the United States: Canadian and Mexican pollution influences, Atmos. Environ., 43(6), 1310–

650   1319, doi:10.1016/j.atmosenv.2008.11.036, 2009.

Van Der Werf, G. R., Randerson, J. T., Giglio, L., Collatz, G. J., Mu, M., Kasibhatla, P. S., Morton, D. C., Defries, R. S., Jin, Y. and Van Leeuwen, T. T.: Global fire emissions and the contribution of deforestation, savanna, forest, agricultural, and peat fires (1997-2009), Atmos. Chem. Phys., 10(23), 11707–11735, doi:10.5194/acp-10-11707-2010, 2010.

655   Xiao, Y., Logan, J. A., Jacob, D. J., Hudman, R. C., Yantosca, R. and Blake, D. R.: Global budget of ethane and regional constraints on U.S. sources, J. Geophys. Res., 113(D21), D21306, doi:10.1029/2007JD009415, 2008.

Yang, J., Tian, H., Tao, B., Ren, W., Pan, S., Liu, Y. and Wang, Y.: A growing importance of large fires in conterminous United States during 1984-2012, J. Geophys. Res. G Biogeosciences, 120(12), 2625–2640, doi:10.1002/2015JG002965, 2015.

660 Yevich, R. and Logan, J. A.: An assessment of biofuel use and burning of agricultural waste in the developing world, Global Biogeochem. Cycles, 17(4), n/a-n/a, doi:10.1029/2002GB001952, 2003.

Young, P. J., Naik, V., Fiore, A. M., Gaudel, A., Guo, J., Lin, M. Y., Neu, J., Parrish, D. D., Rieder, H. E., Schnell, J. L., Tilmes, S., Wild, O., Zhang, L., Brandt, J., Delcloo, A., Doherty, R. M., Geels, C., Hegglin, M. I., Hu, L., Im, U., Kumar, R., Luhar, A., Murray, L. T., Plummer, D., Rodriguez, J., Saiz-Lopez, A., Schultz, M. G., Woodhouse,

665 M., Zeng, G. and Ziemke, J.: Tropospheric Ozone Assessment Report (TOAR): Assessment of global-scale model performance for global and regional ozone distributions, variability, and trends, Elem. Sci. Anthr., 0–84 [online] Available from: http://eprints.lancs.ac.uk/88836/1/TOAR_Model_Performance_07062017.pdf (Accessed 12 December 2017), 2017.

Yu, K., Jacob, D. J., Fisher, J. A., Kim, P. S., Marais, E. A., Miller, C. C., Travis, K. R., Zhu, L., Yantosca, R. M.,

670 Sulprizio, M. P., Cohen, R. C., Dibb, J. E., Fried, A., Mikoviny, T., Ryerson, T. B., Wennberg, P. O. and Wisthaler, A.: Sensitivity to grid resolution in the ability of a chemical transport model to simulate observed oxidant chemistry under high-isoprene conditions, Atmos. Chem. Phys, 16, 4369–4378, doi:10.5194/acp-16-4369-2016, 2016.

Zhang, L., Jacob, D. J., Downey, N. V., Wood, D. A., Blewitt, D., Carouge, C. C., van Donkelaar, A., Jones, D. B. A., Murray, L. T. and Wang, Y.: Improved estimate of the policy-relevant background ozone in the United States

675 using the GEOS-Chem global model with $1/2° \times 2/3°$ horizontal resolution over North America, Atmos. Environ., 45(37), 6769–6776, doi:10.1016/j.atmosenv.2011.07.054, 2011.

Zhang, L., Jacob, D. J., Yue, X., Downey, N. V., Wood, D. A. and Blewitt, D.: Sources contributing to background surface ozone in the US Intermountain West, Atmos. Chem. Phys., 14(11), 5295–5309, doi:10.5194/acp-14-5295-2014, 2014.

680

Figures

Table 1: Sensitivity simulations with the GEOS-Chem model and their application to estimate sources of ground-level O$_3$.

Ozone Source	*Definition*	*Notation*
Base	Standard simulation	O$_3$_Base
Natural Background	Simulation with no global anthropogenic emissions + preindustrial CH$_4$ levels	O$_3$_NAT
North American Background	Simulation with no North American anthropogenic emissions	O$_3$_NAB
U.S. Background	Simulation with no U.S. anthropogenic emissions	O$_3$_USB
U.S. Anthropogenic Emissions	O$_3$_Base – O$_3$_USB	O$_3$_USA
Anthropogenic Emissions from Canada and Mexico	O$_3$_USB – O$_3$_NAB	O$_3$_CA+MX
Intercontinental Transport + Preindustrial CH$_4$ Levels	O$_3$_NAB – O$_3$_NAT	O$_3$_ICT+CH$_4$
North American Lightning NO$_x$	O$_3$_Base – simulation with the lightning NO$_x$ source shut off	O$_3$_NALNO$_x$
Soil NO$_x$ Emissions	O$_3$_Base – simulation with the soil NO$_x$ emissions shut off	O$_3$_SNO$_x$
Terrestrial Biogenic VOC Emissions	O$_3$_Base – simulation with the terrestrial biogenic emissions shut off	O$_3$_BVOC
All Emissions except Terrestrial Biogenic VOCs	Simulation with terrestrial biogenic VOC emissions shut off	O$_3$_noBVOC
Biomass Burning Emissions	O$_3$_Base – simulation with biomass burning emissions (NO$_x$, CO, VOCs, aerosols, and precursors from fires) shut off	O$_3$_BB

685
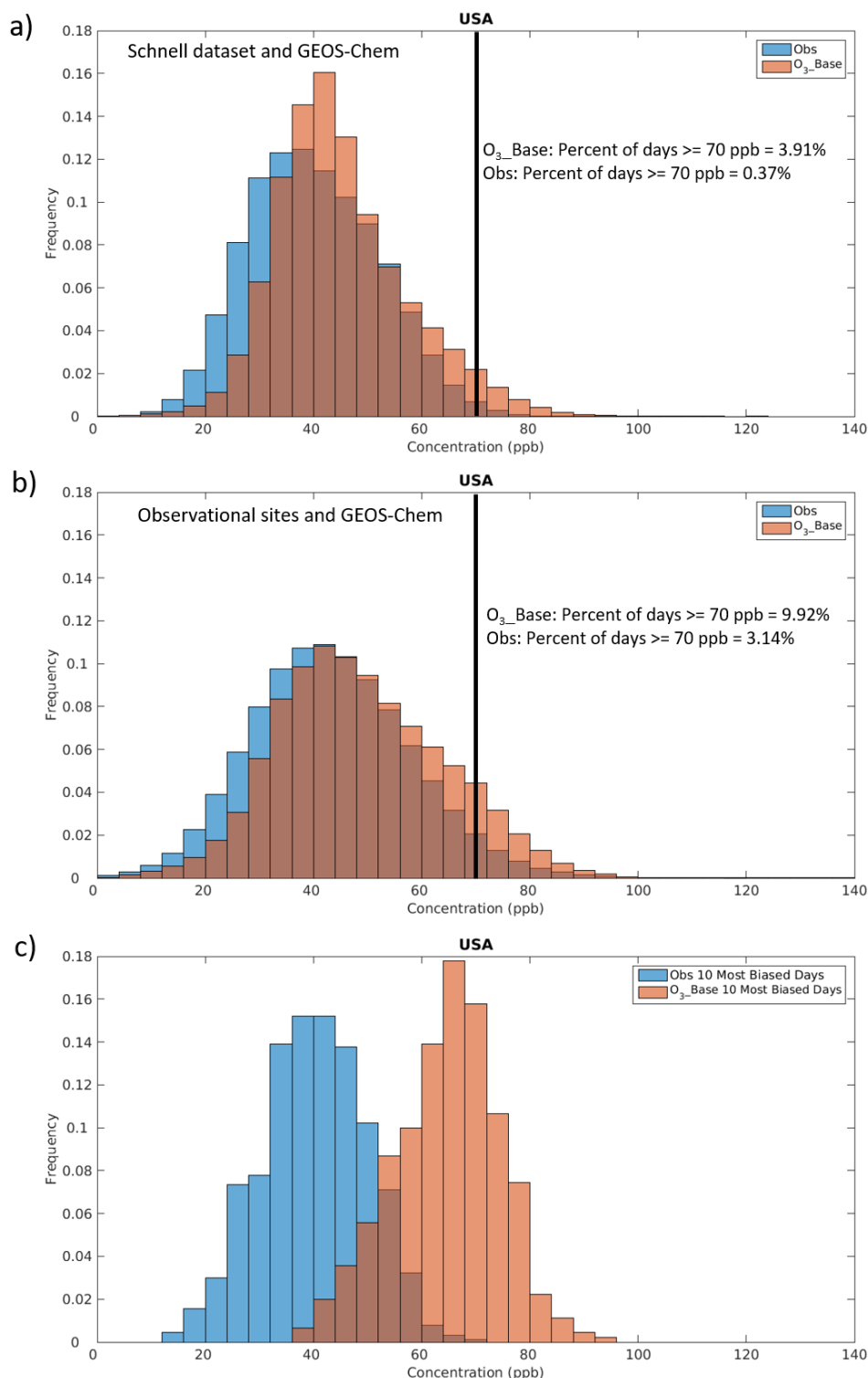
Figure 1: Frequency distribution of regionally averaged U.S. MDA8 O_3 values from 2004-2012 in the (a) Schnell and Prather (2017) dataset interpolated to 2° by 2.5° and (b) at individual observational sites prior to averaging over each of the 10 EPA regions (total number of points is 9 years x 365 or 366 days x 10 regions) in the observations (blue) and the GEOS-Chem model (orange). c) As in panel (b) but selecting for the 10 most biased days in each region (total number of points is 9 years x 10 days x 10 regions). The line drawn at 70 ppb in panels (a) and (b) is the current O_3 NAAQS level.

690
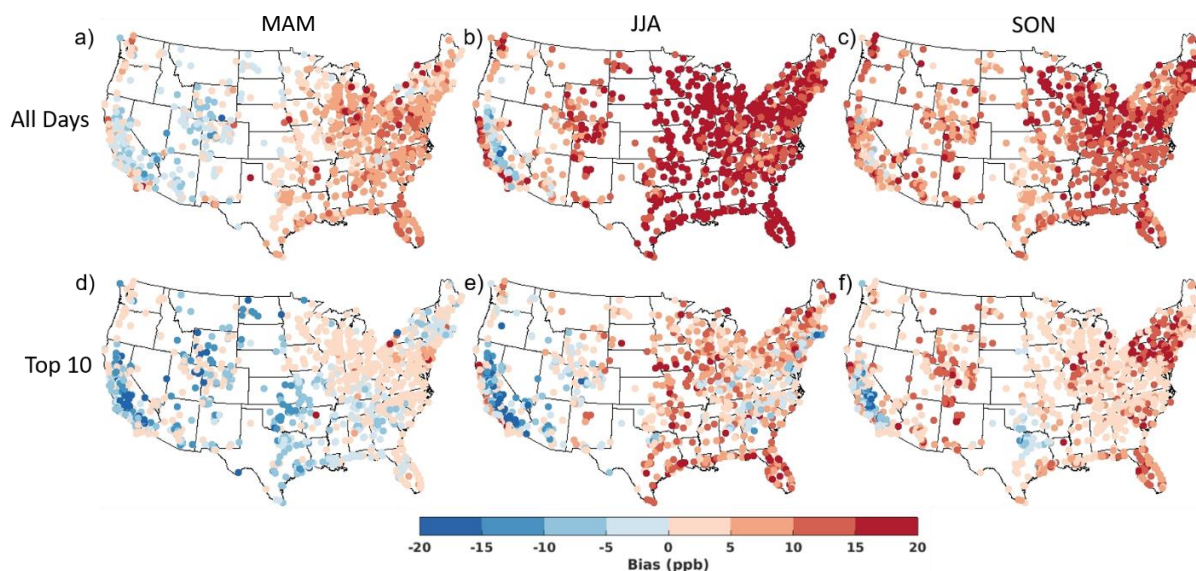
Figure 2: Average MDA8 O₃ model bias (O₃_Base – observed) on all days in (a)MAM, (b) JJA, and (c) SON versus on the (d) O₃_top10obs_MAM, (e) O₃_top10obs_JJA, and (f) O₃_top10obs_SON days at each observational site averaged across 2004-2012.

695
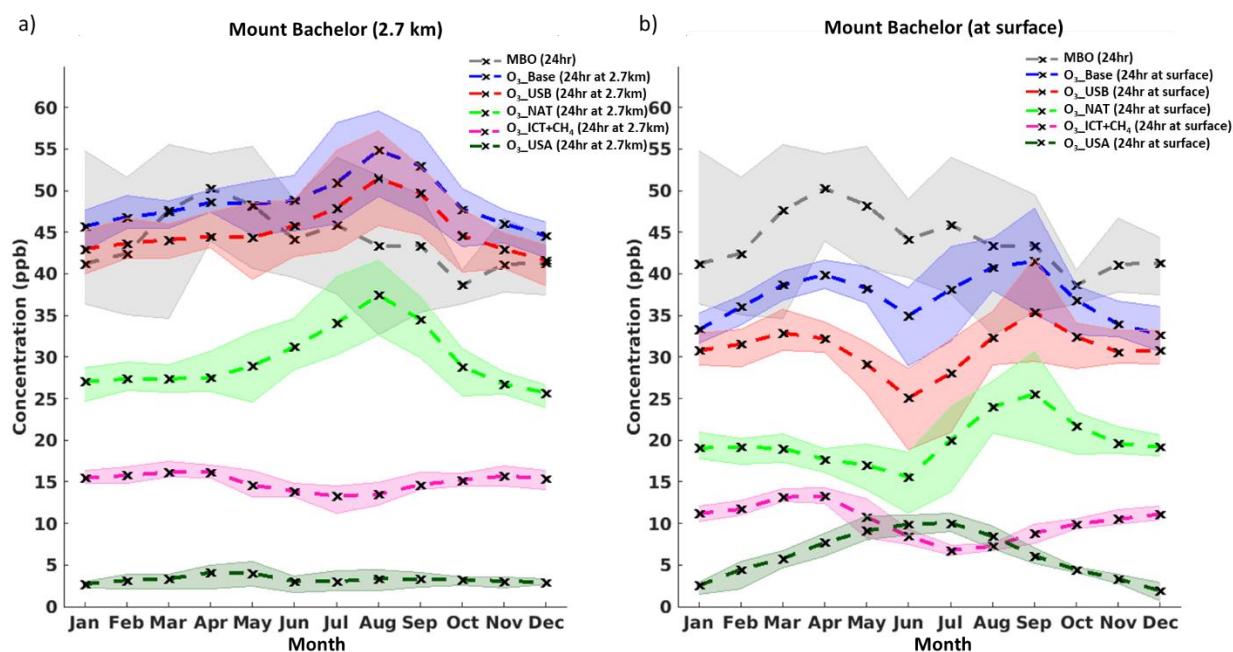
Figure 3: Monthly 2004-2012 average 24-hour O₃ concentrations at Mount Bachelor Observatory. Observations (grey) are the same in both panels. Simulations from the GEOS-Chem model are sampled in the grid cell containing Mount Bachelor at (a) 2.7 km (the height of the Mount Bachelor Observatory) and at (b) the surface: O₃_Base (blue), O₃_USB (red), O₃_NAT (light green), O₃_ICT+CH₄ (pink), and O₃_USA (dark green). The shaded range spans the highest and lowest years.

700
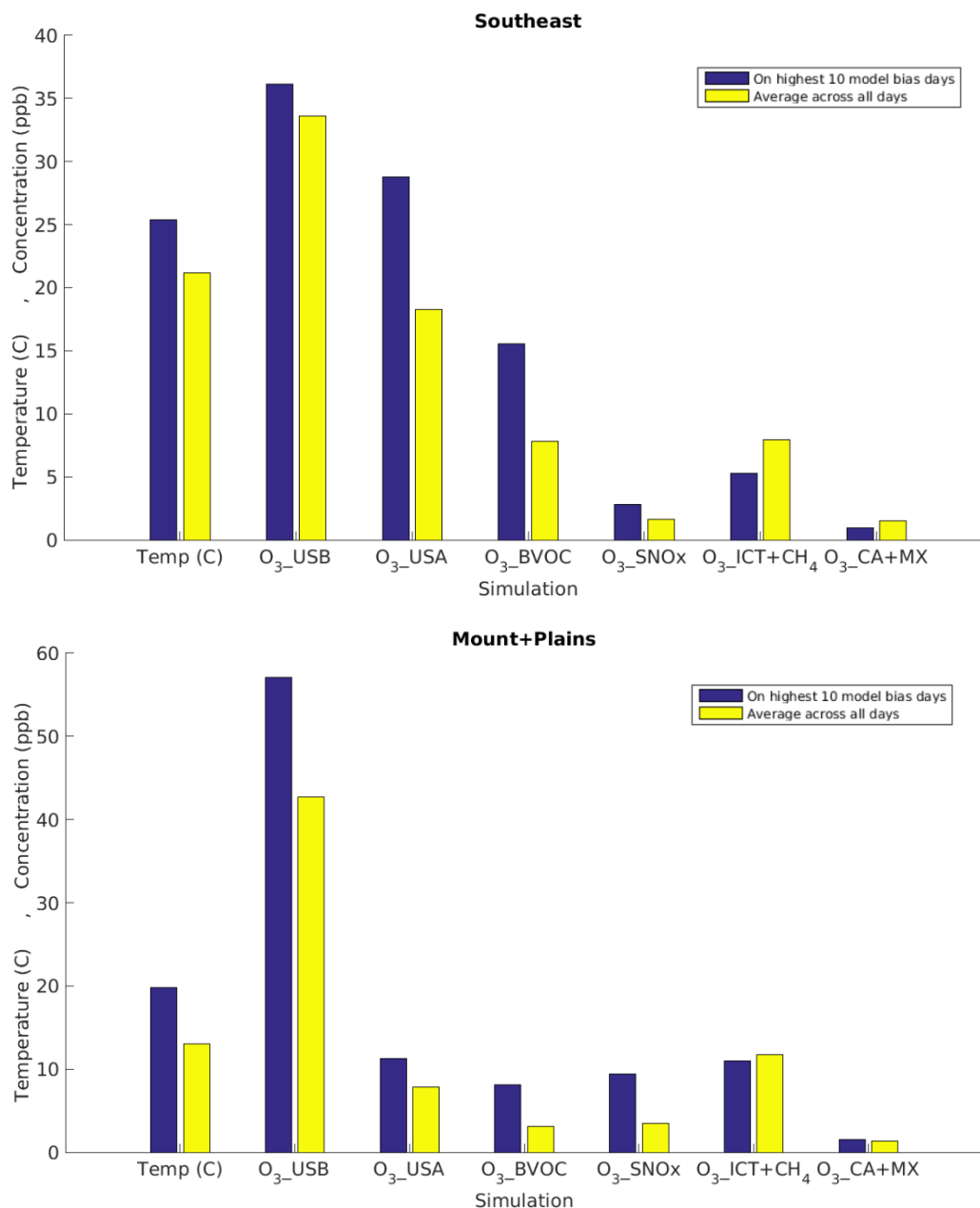
Figure 4: Multi-year (2004-2012) Mar-Oct average temperature and MDA8 O₃ source contributions estimated with the GEOS-Chem model in the (a) Southeast and (b) Mountain and Plains regions on the 10 most biased days (blue) versus averaged across all days (yellow). Note that the two regions are on different scales.

705

710

Table 2: Summary information for each region. The "Model Bias" column shows the model bias in each region on the (1) O$_3$_top10obs days in each season (average of 2004-2012), 2) across all days in each season (average of 2004-2012), and (3) the difference between these values, rounded to the nearest whole number. The other columns show the concentration for the observations, O$_3$_Base, and O$_3$_USA, and daily average temperature (in degrees C) on the (1) O$_3$_top10obs days in each season (average of 2004-2012), (2) across all days in each season (average of 2004-2012), and (3) the difference between these values.

Region	Metric / Season	Model Bias			O$_3$_Base			Obs			O$_3$_USB			O$_3$_USA			Temperature (C)		
		MAM	JJA	SON	MAM	JJA	SON	MAM	JJA	SON	MAM	JJA	SON	MAM	JJA	SON	MAM	JJA	SON
New England	Top 10 Days	-1	9	12	57	72	59	58	62	59	35	39	36	22	33	23	12	22	18
	Avg all days	2	14	10	46	56	41	44	43	31	35	35	32	12	21	9	7	19	11
	Difference	-3	-4	2	11	16	18	13	20	28	0	4	3	10	11	14	5	2	6
NY+NJ	Top 10 Days	4	14	15	63	80	65	59	67	65	36	42	38	27	38	27	16	24	20
	Avg all days	5	18	11	49	65	42	44	47	31	35	39	33	14	27	10	9	21	12
	Difference	-1	-5	4	14	15	23	15	19	34	1	3	6	13	11	18	6	2	7
Mid-Atlantic	Top 10 Days	3	13	15	65	81	69	63	68	69	34	40	37	31	40	32	18	25	21
	Avg all days	6	18	12	51	70	45	46	52	33	34	38	32	17	32	13	12	23	14
	Difference	-3	-5	3	14	11	24	17	16	36	0	2	5	14	9	19	6	2	7
Southeast	Top 10 Days	0	13	10	62	72	63	61	59	63	34	39	34	27	34	28	19	26	21
	Avg all days	6	19	12	55	65	51	48	46	39	34	37	32	21	28	19	17	26	18
	Difference	-6	-6	-1	7	7	12	13	13	24	1	2	3	7	5	10	2	1	3
Midwest	Top 10 Days	4	14	17	63	77	70	59	63	70	36	44	42	27	33	27	17	24	21
	Avg all days	6	19	11	49	68	43	44	48	32	34	42	33	15	26	10	10	22	12
	Difference	-1	-5	6	14	10	26	15	15	37	1	2	9	12	8	17	7	1	9
South Central	Top 10 Days	0	13	9	60	75	67	60	62	67	39	45	40	21	30	26	20	27	23
	Avg all days	5	17	10	52	62	51	47	46	41	36	41	35	16	21	16	18	27	19
	Difference	-5	-4	-2	8	12	15	14	16	26	3	4	5	6	9	10	2	1	4
Plains	Top 10 Days	0	13	13	58	74	67	58	61	67	37	47	42	21	28	25	17	26	22
	Avg all days	5	18	10	50	67	45	44	49	35	34	44	34	15	23	11	13	25	13
	Difference	-6	-5	3	8	8	23	14	13	33	2	3	9	6	5	14	4	1	9
Mountains + Plains	Top 10 Days	-1	8	13	56	69	64	57	60	64	45	57	54	11	12	10	12	22	18
	Avg all days	0	11	9	50	64	48	50	53	39	41	53	41	10	11	7	7	20	9
	Difference	-1	-2	4	6	5	16	7	7	25	5	4	12	1	0	3	5	2	9
Pacific SW	Top 10 Days	-3	3	6	57	64	63	60	62	63	41	47	48	16	18	15	18	25	24
	Avg all days	0	4	8	49	57	49	49	53	42	37	41	39	12	16	10	14	23	17
	Difference	-3	-1	-2	8	7	14	10	9	21	4	6	8	4	2	5	5	2	7
Pacific NW	Top 10 Days	-1	6	11	48	59	51	49	52	51	39	49	44	9	10	7	12	22	17
	Avg all days	2	8	10	43	46	40	41	38	30	35	36	36	8	10	4	8	17	10
	Difference	-3	-2	0	5	13	11	9	14	21	4	12	9	1	0	3	4	4	7

715

Table 3: Summary information for each region. Each column shows the concentration for each background O₃ source influence on the (1) O₃_top10obs days in each season (average of 2004-2012), (2) across all days in each season (average of 2004-2012), and (3) the difference between these values, rounded to the nearest whole number.

Region	Metric / Season	O₃_USB MAM	JJA	SON	O₃_BVOC MAM	JJA	SON	O₃_SNOx MAM	JJA	SON	O₃_NALNOx MAM	JJA	SON	O₃_ICT+CH₄ MAM	JJA	SON	O₃_CA+MX MAM	JJA	SON
New England	Top 10 Days	35	39	36	6	17	13	1	3	2	1	2	1	8	3	5	7	7	5
	Avg all days	35	35	32	2	10	6	1	3	2	1	2	2	10	4	7	6	6	4
	Difference	0	4	3	4	7	8	0	0	1	0	0	0	-2	-1	-3	1	1	2
NY+NJ	Top 10 Days	36	42	38	9	20	17	1	4	3	1	2	2	7	2	4	6	6	5
	Avg all days	35	39	33	3	14	7	1	3	2	1	2	2	10	4	7	5	6	4
	Difference	1	3	6	6	6	9	0	0	1	0	0	0	-2	-1	-3	1	0	2
Mid-Atlantic	Top 10 Days	34	40	37	10	20	18	1	4	3	1	3	2	7	3	5	4	3	4
	Avg all days	34	38	32	5	16	9	1	3	2	1	3	2	9	4	7	4	4	3
	Difference	0	2	5	5	4	9	0	1	1	0	0	0	-2	-1	-2	0	0	1
Southeast	Top 10 Days	34	39	34	7	16	14	2	4	2	1	3	2	8	4	6	2	2	2
	Avg all days	34	37	32	5	14	9	1	3	2	2	4	2	9	5	7	2	1	2
	Difference	1	2	3	2	2	4	0	1	1	-1	-1	0	0	-1	-1	0	1	0
Midwest	Top 10 Days	36	44	42	8	16	16	2	6	5	1	2	2	6	1	4	3	3	3
	Avg all days	34	42	33	3	13	8	1	6	2	1	2	2	9	2	6	4	3	2
	Difference	1	2	9	4	3	8	1	0	2	0	0	0	-3	-1	-3	0	0	1
South Central	Top 10 Days	39	45	40	6	17	14	3	5	4	2	4	2	8	5	6	3	2	2
	Avg all days	36	41	35	4	12	8	2	4	2	2	6	2	9	7	8	3	2	2
	Difference	3	4	5	2	5	6	1	1	2	0	-2	0	-1	-2	-2	0	0	0
Plains	Top 10 Days	37	47	42	5	16	14	3	8	6	1	3	2	7	2	4	3	1	1
	Avg all days	34	44	34	3	13	7	2	8	3	1	3	2	8	3	7	3	2	2
	Difference	2	3	9	2	3	7	1	0	3	0	0	0	-1	-1	-2	0	0	0
Mountains + Plains	Top 10 Days	45	57	54	1	8	7	3	9	7	3	5	5	12	11	12	2	1	1
	Avg all days	41	53	41	1	7	4	2	8	3	2	5	4	12	11	12	2	2	1
	Difference	5	4	12	1	1	3	1	1	4	1	0	1	0	1	1	0	0	0
Pacific SW	Top 10 Days	41	47	48	3	9	9	3	5	5	2	4	4	11	8	10	2	2	2
	Avg all days	37	41	39	1	7	5	1	4	3	2	4	3	12	8	11	1	2	2
	Difference	4	6	8	2	2	4	1	1	2	0	0	1	-1	0	-1	0	0	0
Pacific NW	Top 10 Days	39	49	44	0	9	7	2	7	5	1	3	3	12	9	10	3	4	2
	Avg all days	35	36	36	-1	4	3	1	4	2	1	2	3	13	9	10	2	3	1
	Difference	4	12	9	1	5	4	1	3	3	0	1	0	0	0	0	1	1	1
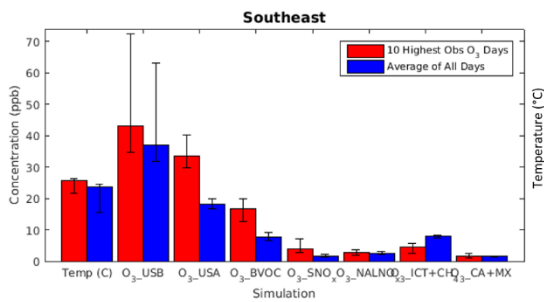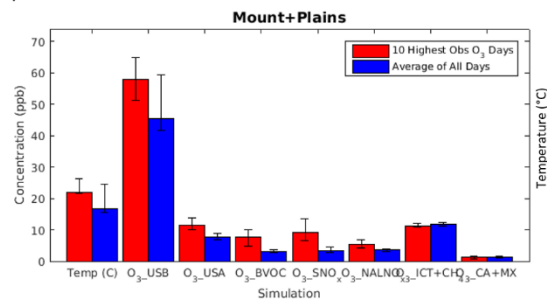
Figure 5: Average 2004-2012 influence of each sensitivity simulation to O₃_Base in the (a) Southeast and (b) Mountains and Plains regions on MDA8 O₃_top10obs_JJA days (red) versus averaged across all days (blue). Error bars show the concentration on the lowest versus highest year for each sensitivity simulation in each region.
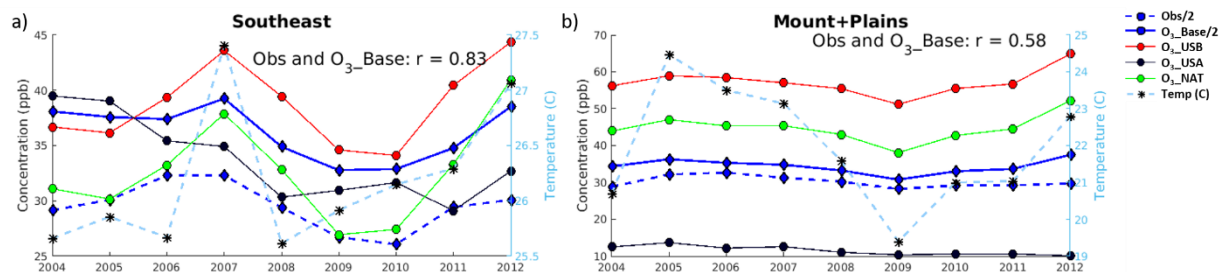
Figure 6: Average yearly MDA8 O₃_top10obs_JJA concentrations for observations (divided by 2 to fit on the same axes; blue dashed line), O₃_Base (divided by 2; blue solid line), O₃_USB (red), O₃_USA (black), O₃_NAT (green) MDA8, and daily average temperature (in degrees C; light blue) in the (a) Southeast and (b) Mountains and Plains regions.

Table 4: Change in MDA8 O₃ concentrations from 2004-2006 to 2010-2012 on O₃_top10obs_JJA days in the observations, O₃_Base, O₃_USB, O₃_USA, and temperature.

	Obs	O₃_Base	O₃_USB	O₃_USA	Temperature (C)
New England	-6	-4	6	-10	2
NY+NJ	-2	-4	3	-7	1
Mid-Atlantic	0	-3	4	-7	1
Southeast	-4	-5	2	-7	1
Midwest	-2	-4	2	-6	0
South Central	-6	-2	5	-7	1
Plains	-1	-2	4	-5	1
Mountains + Plains	-4	-1	1	-2	-1
Pacific SW	-3	-4	0	-4	-1
Pacific NW	-7	-5	-4	-1	-1
Average	*-3*	*-3*	*2*	*-6*	*0*

730
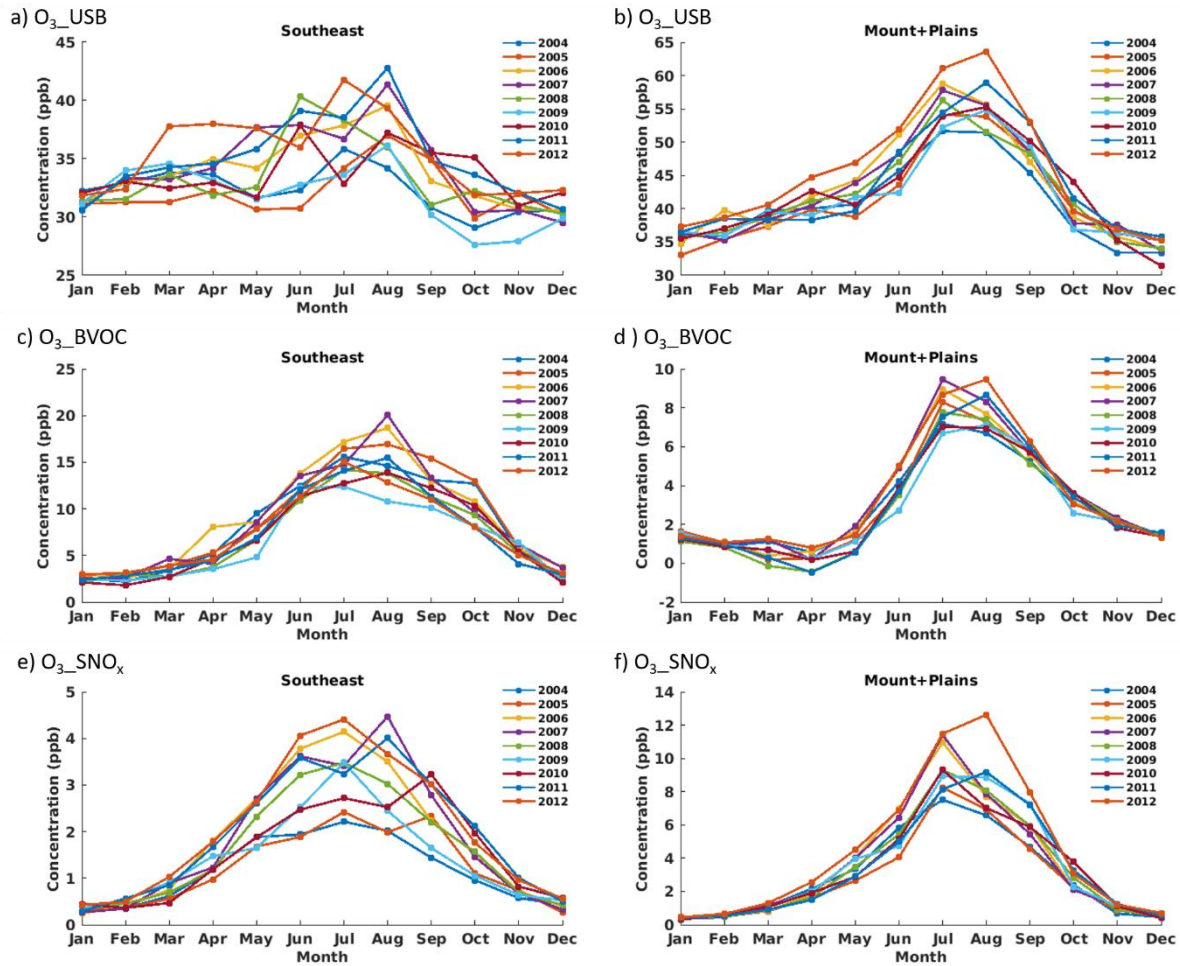
735 **Figure 7: Monthly average MDA8 O₃_USB (a, b), O₃_BVOC (c, d), and O₃_SNOₓ (e, f) concentrations in the Southeast (a, c, e) and Mountains and Plains (b, d, f) regions.**
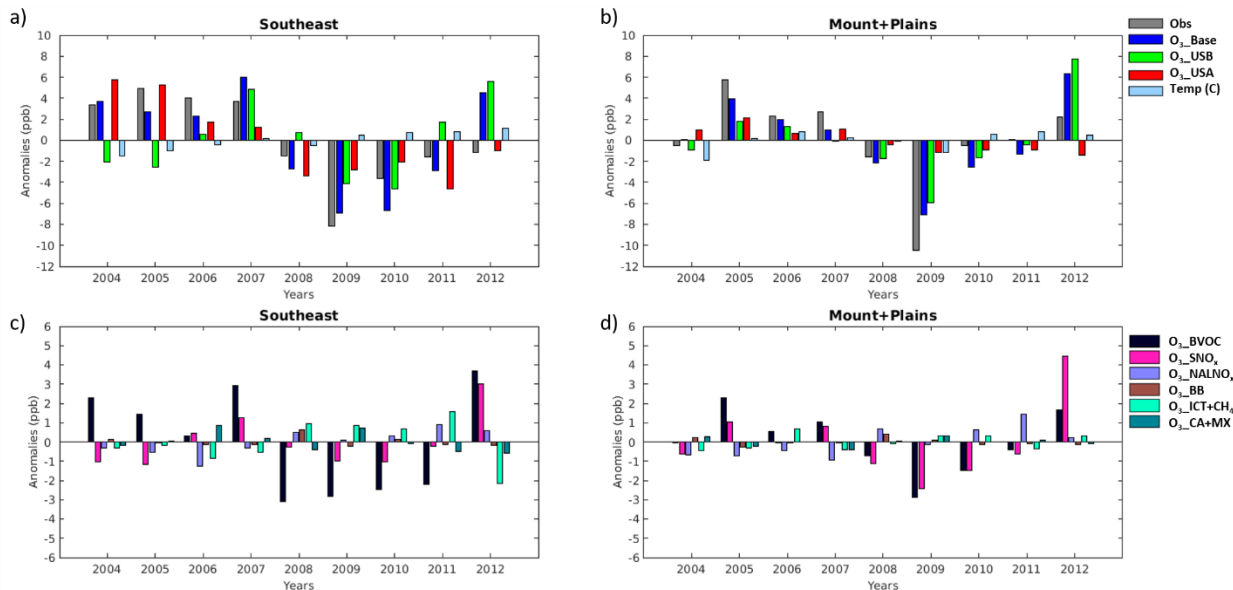
Figure 8: Anomaly on the MDA8 O₃_top10obs_JJA days relative to the 2004-2012 average in the Southeast (a, c) and in the Mountains and Plains (b, d) regions. Panels (a) and (b) show the observations, O₃_Base, O₃_USB, O₃_USA, and temperature (in degrees C). Panels (c) and (d) show O₃_BVOC, O₃_SNOₓ, O₃_NALNOₓ, O₃_BB, O₃_ICT+CH₄, and O₃_CA+MX.
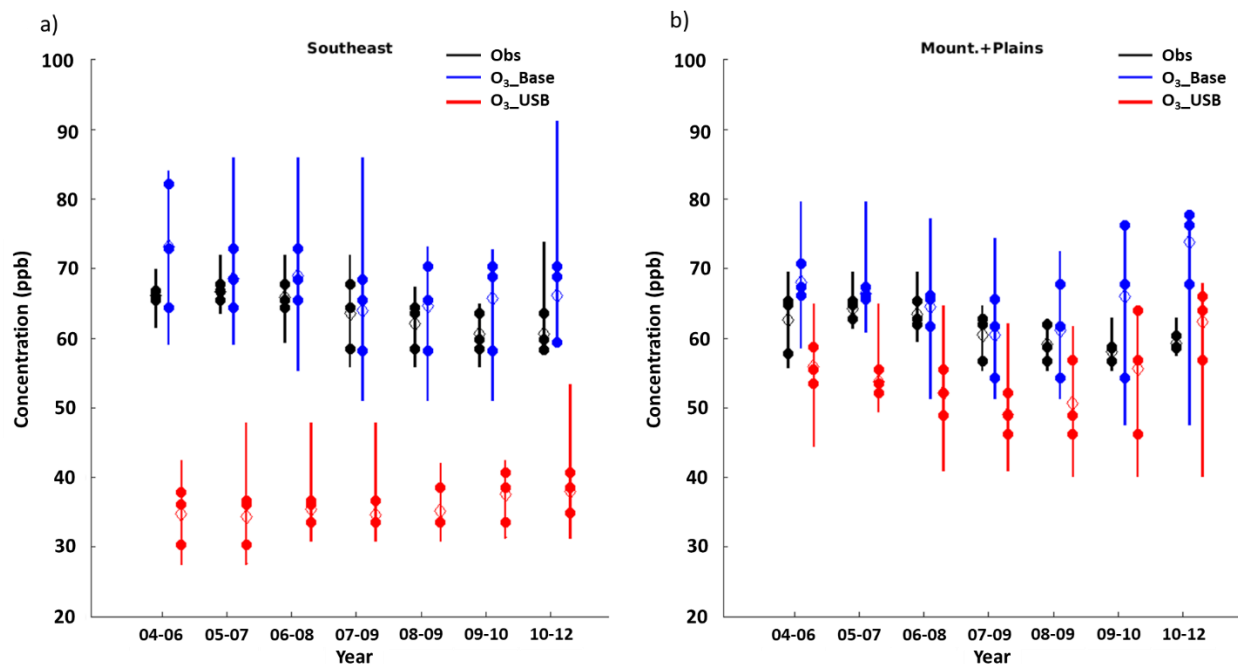
Figure 9: The three 4th highest days in each year (solid dots) that went into the calculation of the three-year average of the 4th highest MDA8 O₃ day (hollow diamond). Error bars show the range between the highest and lowest O₃_top10obs days across each 3-year span (i.e, across 30 total points) occurring between March and October in the (a) Southeast and (b) Mountains and Plains regions in the observations (black), and the O₃_Base (blue) and O₃_USB (red) simulations sampled on the same days as the top 10 observed values.

Table 5: Summary information for each region. The first row next to each region reports the range across 2004-2012 of the 4th highest values from each of the 9 individual years for the observations, O₃_Base, and O₃_USB. The second row reports the range across 2004-2012 of each of the 3-year averages of the 4th highest values (7 values) in each region for the observations, O₃_Base, and O₃_USB.

Region	Range	Obs	O_3_Base	O_3_USB
New England	4th highest day	15	16	10
	3-year average 4th highest day	9	10	3
	Difference	**-6**	**-6**	**-7**
NY+NJ	4th highest day	11	10	12
	3-year average 4th highest day	6	2	6
	Difference	**-5**	**-8**	**-6**
Mid-Atlantic	4th highest day	13	36	25
	3-year average 4th highest day	7	21	10
	Difference	**-6**	**-15**	**-15**
Southeast	4th highest day	9	24	10
	3-year average 4th highest day	6	9	4
	Difference	**-3**	**-15**	**-7**
Midwest	4th highest day	13	22	24
	3-year average 4th highest day	8	11	10
	Difference	**-6**	**-11**	**-14**
South Central	4th highest day	11	26	22
	3-year average 4th highest day	8	13	13
	Difference	**-3**	**-13**	**-9**
Plains	4th highest day	14	32	24
	3-year average 4th highest day	9	18	11
	Difference	**-5**	**-15**	**-13**
Mountains + Plains	4th highest day	9	23	20
	3-year average 4th highest day	6	13	13
	Difference	**-2**	**-10**	**-7**
Pacific SW	4th highest day	5	23	20
	3-year average 4th highest day	3	5	5
	Difference	**-2**	**-18**	**-15**
Pacific NW	4th highest day	11	14	15
	3-year average 4th highest day	5	9	12
	Difference	**-5**	**-5**	**-3**